PHILOSOPHICAL TRANSACTIONS A

royalsocietypublishing.org/journal/rsta

Research

Cite this article: Miramirkhani F, Uysal M. 2020 Channel modelling for indoor visible light communications. *Phil. Trans. R. Soc. A* **378**: 20190187.
http://dx.doi.org/10.1098/rsta.2019.0187

Accepted: 10 January 2020

One contribution of 17 to a theme issue 'Optical wireless communication'.

Subject Areas:
electrical engineering

Keywords:
visible light communications, channel modelling, optical communication, communication systems

Author for correspondence:
Murat Uysal
e-mail: murat.uysal@ozyegin.edu.tr

Channel modelling for indoor visible light communications

Farshad Miramirkhani[1] and Murat Uysal[2]

[1]Department of Electrical and Electronics Engineering, Isik University, 34980 Istanbul, Turkey
[2]Department of Electrical and Electronics Engineering, Ozyegin University, 34794 Istanbul, Turkey

FM, 0000-0002-6691-9779; MU, 0000-0001-5945-0813

Visible light communication (VLC) allows the dual use of light-emitting diodes (LEDs) for wireless communication purposes in addition to their primary purpose of illumination. As in any other communication system, realistic channel modelling is a key for VLC system design, analysis and testing. In this paper, we present a comprehensive survey of indoor VLC channel models. In order to set the background, we start with an overview of infrared (IR) channel modelling, which has received much attention in the past, and highlight the differences between visible and IR optical bands. In the light of these, we present a comparative discussion of existing VLC channel modelling studies and point out the relevant advantages and disadvantages. Then, we provide a detailed description of a site-specific channel modelling approach based on non-sequential ray tracing that precisely captures the optical propagation characteristics of a given indoor environment. We further present channel models for representative deployment scenarios developed through this approach that were adopted by the Institute of Electrical and Electronics Engineering (IEEE) as reference channel models. Finally, we consider mobile VLC scenarios and investigate the effect of receiver location and rotation for a mobile indoor user.

This article is part of the theme issue 'Optical wireless communication'.

1. Introduction

It is estimated that around 70–80% of mobile data traffic takes place in an indoor environment [1]. This requires the development of low-cost, energy-efficient

THE ROYAL SOCIETY PUBLISHING

and high-speed indoor wireless access solutions. To release the pressure on the highly congested radiofrequency (RF) spectrum, visible light communication (VLC) has emerged as a complementary and/or alternative wireless access technology [2–4]. VLC is based on the principle of modulating light-emitting diodes (LEDs) at very high speeds that are not noticed by human eye. This allows the use of LED luminaires for wireless communication in addition to their primary function of illumination. Operating at optical bands with large bandwidth capacity, VLC can be used as a complementary technology where excess capacity demands of cellular or Wi-Fi networks can be offloaded. VLC can be potentially used as an alternative in safety-critical and hostile environments such as hospitals, airplanes, petrochemical plants, mines, where the use of RF is prohibited or partially restricted.

In recent years, there has been a surge of research activities in VLC in both academic and industrial circles which has led to a well-established literature on VLC, e.g. comprehensive surveys [5–12]. Initial works mostly focused on point-to-point links and physical layer development. VLC relies on intensity modulation and direct detection (IM/DD) where the information is encoded in the intensity of LED light and then retrieved through a photodetector (PD) at the receiver. In IM/DD, the information waveform that modulates the light intensity must be non-negative and real valued. In order to satisfy these conditions, simple modulation techniques such as on–off keying (OOK), pulse place modulation (PPM) and pulse width modulations (PWM) have been studied in earlier works [13–15].

The multipath characteristics of VLC channel combined with the low-pass natures of LED and front-end limit the available electrical bandwidth. To mitigate the effects of intersymbol interference (ISI) over frequency-selective VLC channels, more recent works adopted multicarrier transmission with a particular focus on orthogonal frequency division multiplexing (OFDM), e.g. [16–19]. Several variants of optical OFDM were proposed to comply with the requirement that the LED driving signal should be non-negative and real valued. Advanced techniques such as adaptive transmission [20–22], relay-assisted transmission [23–25] and multiple-input multiple-output (MIMO) communications [26–28] were further explored in the context of VLC. More recent works focused on upper layer solutions to transform VLC into a multi-user, scalable and fully networked wireless technology. These address medium access [29,30], interference management [31], handover techniques [32] and resource allocation [33].

Similar to any wireless communication system, the propagation channel as well as the characteristics of transmitter/receiver front-ends dictate the fundamental limits on the physical layer performance of VLC system. Realistic propagation channel models are therefore of critical importance for VLC system design, performance evaluation and testing and will be the focus of our paper. While most of earlier works assumed simple line-of-sight (LOS) channel model, there have been significant research efforts to develop more accurate VLC channel models [5,7,34]. In this paper, we first present a comprehensive survey of the existing indoor VLC channel models and then present some new results on the effect of photodetector location for an indoor mobile VLC channel.

In order to set the background for VLC channel modelling, §2 starts with an overview of infrared (IR) channel modelling which has received much attention in the past [35–46]. Both recursive calculation methods [35–39] and geometric-based models [40–42] were used to obtain IR channel models. As an alternative to deterministic methods, Monte Carlo ray tracing (MCRT) and its modified version were also used in IR channel modelling [43–46]. Unlike monochromatic IR sources, a white light LED source is inherently wideband. Furthermore, the reflectance of most materials in the visible light (VL) spectrum significantly varies while this remains typically constant within IR band. Owing to such fundamental differences, the IR channel models cannot be applied to VLC channel modelling in a straightforward manner. This requires the development of dedicated VLC channel models.

In §2, we further review earlier works in this area [47–57] which have built on some simplifying yet idealistic assumptions, such as ideal Lambertian sources, purely diffuse reflections and empty room. To address these issues, we have developed a site-specific channel modelling approach in our earlier works [34,58,59] where accelerated ray tracing is used to obtain channel impulse

responses (CIRs) for various indoor environments. In §3, we describe this approach in detail which is able to obtain CIRs for any non-ideal source types as well as specular and mixed specular-diffuse reflections. Furthermore, a large number of reflections (more than 10) can be easily handled for better accuracy. Our approach represents the state of the art in the field and the indoor VLC channel models developed through this approach were adopted by IEEE as reference channel models [34] elaborated in §4.

Most of the existing works in VLC channel modelling assume static scenarios where transmitter and receiver are located at fixed points. In practice, user mobility should be taken into account as well as the effect of photodetector location/orientation. Towards this, in §5, we consider a mobile receiver terminal in the form of a cell phone. Seven possible locations are considered for the photodetector. Five of these are on the top edge and two of them are on the top round corners of the device. For each possible location of photodetector, we obtain CIRs and corresponding path loss. To further demonstrate the effects of user location, we present the spatial distribution of channel gain within the room. We present concluding remarks in §6.

2. Optical channel modelling

In this section, we first provide an overview of IR channel modelling which has been the inspiration point for most works in VLC. Then, we discuss the differences between VL and IR bands highlighting the need for the development of dedicated VLC channels.

(a) Deterministic and non-deterministic modelling

Optical channel modelling approaches can be roughly categorized in two main classes as deterministic and non-deterministic. Recursive calculation [35–39] and geometric-based models [40–42] are the most widely used deterministic techniques while MCRT [43–46] represents the non-deterministic approach.

In recursive method [36], the surfaces of indoor environment (i.e. walls, floor and ceiling) are discretized into reflecting elements that act as point sources. A single ray from the source is emitted and the ray's bounces are tracked until it reaches detector (figure 1). For each reflection, the received power and corresponding delay are calculated which yields the CIR for that specific reflection. The overall CIR can be then obtained as the summation of CIRs for all reflections. Define $\hat{\mathbf{n}}$ as the normal to the surface at position $\mathbf{r}$. Let $S=\{\mathbf{r}_S, \hat{\mathbf{n}}_S, n\}$ denote the arbitrary source with position of $\mathbf{r}_S$, orientation of $\hat{\mathbf{n}}_S$ and mode number of n. Furthermore, let $R=\{\mathbf{r}_R, \hat{\mathbf{n}}_R, A_R, \mathrm{FOV}\}$ denote the arbitrary receiver with position of $\mathbf{r}_R$, orientation of $\hat{\mathbf{n}}_R$, area of A_R and field of view of FOV. The CIR can be expressed as [36]

$$\begin{aligned} h^{(k)}(t;S,R) &\approx \sum_{i=1}^{N} h^{(0)}(t;S,\varepsilon_i) \otimes h^{(k-1)}(t;\varepsilon_i,R) \\ &= \frac{n+1}{2\pi} \sum_{i=1}^{N} \frac{\rho_i \cos^n(\phi)\cos(\theta)}{d^2} \mathrm{rect}\left(\frac{2\theta}{\pi}\right) h^{(k-1)}\left(\frac{t-d_i}{v}; \{\mathbf{r}, \hat{\mathbf{n}}, 1\}, R\right) \Delta A, \end{aligned} \tag{2.1}$$

where k is the order of reflection; ϵ_i is the ith reflecting element; ρ_i is the reflectivity of the ith reflecting element; ΔA is the area of reflecting element; N is the total number of reflecting elements; ϕ is the irradiance angle; θ is the incident angle; d is the distance between source and receiver and v is the speed of light. In (2.1), $\otimes$ denotes convolution and rect (.) is defined by

$$\mathrm{rect}(x) = \begin{cases} 1 & |x| \le 1 \\ 0 & |x| > 1 \end{cases}. \tag{2.2}$$

Owing to the contribution of multiple reflections, this approach models multipath dispersion with reasonable accuracy [35–39]. However, for reflections of order higher than three, this model proves to be prohibitively expensive in terms of computer memory requirements and total

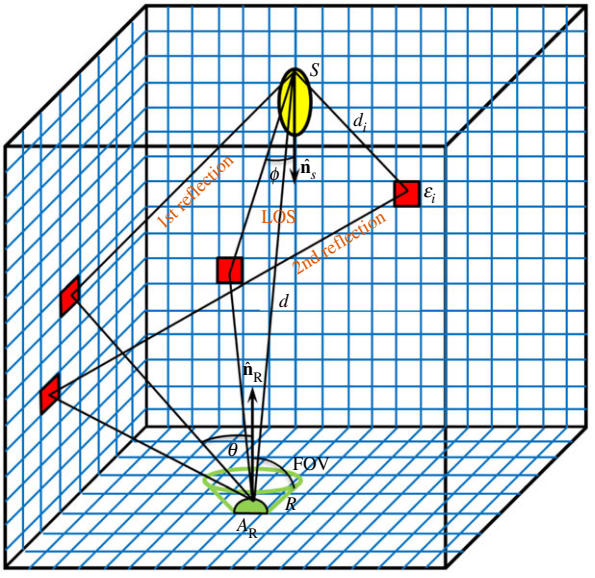

Figure 1. Recursive method. (Online version in colour.)

computation time. To address this issue, several variants of recursive methods were further proposed [37–39]. For example, the DUSTIN algorithm [37] reduces the computational complexity as well as memory requirements by slicing the recursive operations into time steps rather than into a number of reflections. Another alternative is an iterative-based algorithm [39] where CIR calculation follows the basic methodology outlined in [36] with extensions for an arbitrary number of objects inside the environment. It was reported in [39] that the iterative method is more than 90 times faster compared with the recursive method when three reflections are considered.

Another widely used approach is geometric-based modelling, where a closed-form expression for the CIR is constructed by assuming specific transmitter, receiver and reflector geometries. For example, in the so-called ceiling bounce model [40], the transmitter and receiver are co-located in panels parallel to the floor towards the ceiling (figure 2). A closed-form CIR is presented by considering geometric parameters of the room as well as the reflectance values. This model translates the effect of multiple reflections into loss of optical power at the receiver (i.e. path loss) and the delay spread of the signal arriving at the receiver after multiple reflections. In [41], an empty room is considered where the transmitter was placed at the centre of the ceiling and the receiver was placed at a height of 1 m. The indoor CIR is defined as a combination of diffuse components and a direct LOS component. It is shown that at lower frequencies, the diffuse component of the impulse response can be approximated by first-order low-pass frequency response of Ulbricht's integrating sphere. In [42], an empty room is considered where the transmitter and receiver were placed on the floor upward to the ceiling with inter-distance of up to 10 m. As the distance between the source and the receiver increases, the primary reflection impulse responses changes from a sharp shape to a smooth convex shape. As a good match based on curve fitting, the Gamma probability density function is selected in [42] to model the primary reflection impulse response while a spherical model is used to calculate the impulse response associated with higher order reflections. It was further demonstrated that the bandwidth characteristics are dominated by the response of the primary reflection rather than the higher-order reflections.

As an alternative to deterministic methods, MCRT can be employed [43–46]. This approach relies on repeated random sampling to obtain numerical results. In contrast with deterministic methods discussed so far, the Monte Carlo approach allows for the evaluation of the impulse response for environments with complex geometries, especially when a large number of

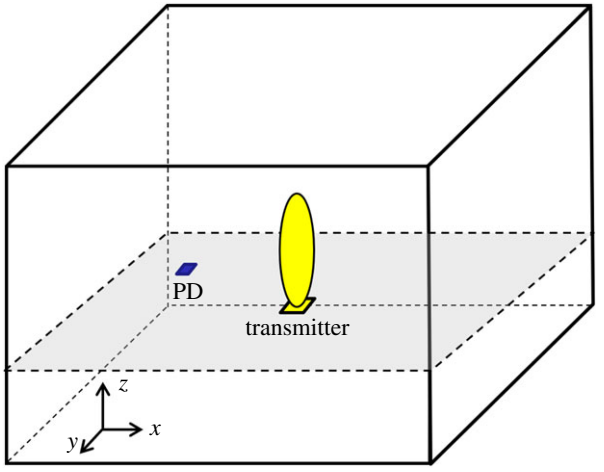

Figure 2. Ceiling bounce model. (Online version in colour.)

reflections are considered. This method involves discretization of room surfaces (i.e. walls, floors, ceiling) into reflecting elements, ray generation based on a given statistical distribution (distribution type depends on the source) and then tracking of each ray until it reaches detector to calculate the detected power and associated delay. In conventional ray tracing algorithms, there is no limitation on the number of reflections that can be considered. However, the probability that the rays will reach the receiver is not high, and so a very large number of rays (i.e. in the order of millions) needs to be traced. To address this issue, accelerated ray tracing algorithms were introduced. For example, in [44], each reflection of the rays is used to calculate an LOS contribution to the receiver from the reflecting point, thus using each ray multiple times instead of only once. This leads to a lower number of generated rays from the source to calculate an impulse response.

(b) Overview of indoor visible light communication channel models

There exist significant differences between VL and IR bands and the IR communication channel models discussed within the previous subsection cannot be applied to VLC channel modelling in a straightforward manner. For example, an IR source can be approximated as a monochromatic emitter while a white light LED source is inherently wideband (380–780 nm) (figure 3). This calls for the inclusion of wavelength dependency of the source in VLC channel modelling [58]. Furthermore, in IR communication, the reflectance of materials is typically modelled as a constant. On the other hand, the reflectance of some materials in the VL spectrum significantly varies (figure 4). Therefore, wavelength dependency should be considered for realistic channel modelling in VLC.

In the early literature, various VLC channel modelling studies were carried out, mainly adopted from earlier works on IR channel modelling including both deterministic [47–54] and non-deterministic approaches [55–57]. For example, in [47], the recursive method proposed in [36] was used to obtain CIR in VL band, but fixed reflectance was assumed. In [48], in an effort to reflect the effect of wavelength dependency in channel modelling, the reflectance values were calculated as the average of wavelength-dependent coefficients over the VL band. In [49], the wavelength dependency, explicitly was taken into account in the recursive method to determine the CIR of an empty room. However, similar to [47,48], the work in [49] was also limited to the assumptions of only purely diffuse reflections and ideal Lambertian source which might not hold true for many practical cases. In [50], a modified version of the recursive method was proposed to integrate the non-ideal Lambertian source with distinct source radiation patterns. In

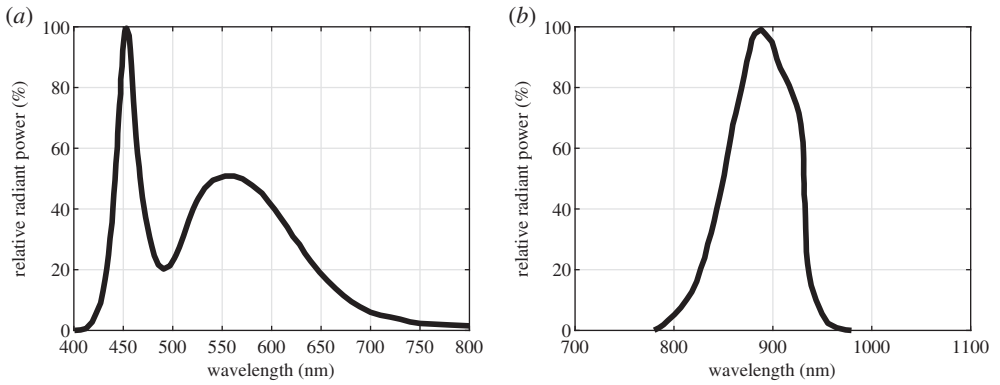

Figure 3. (*a*) Relative spectral power distribution of white LED (Cree Xlamp® MC-E) and (*b*) IR LED (OSRAM® SFH 4283 880 nm).

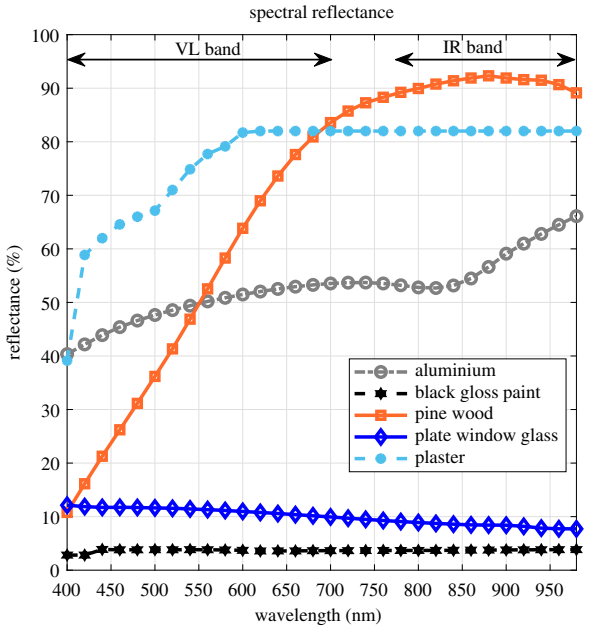

Figure 4. Spectral reflectance of various materials in VL and IR bands. (Online version in colour.)

contrast with time-domain methods, a frequency-domain method was adopted in [51] and the channel transfer functions of diffuse components and LOS component were obtained. Then, a recursive linear time-invariant system was constructed based on the transfer functions.

Geometric-based models were also proposed for VLC channels. Particularly, in [52], a non-line-of-sight (NLOS) analytical channel model for a cuboid room was proposed. In [53], a field of view (FOV) geometry-based single bounce (GBSB) model for VLC channels was developed. Fixed reflectance values with purely diffuse reflections and ideal Lambertian source were assumed in [52,53]. In [54], a regular-shaped geometry-based multiple bounce (RS-GBMB) model for VLC channels was proposed. The proposed model employs a combined two-ring model and ellipse model (see fig. 3 of [54]), where the received signal is constructed as a sum of the LOS, single-, double- and triple bounced rays of different powers.

As an alternative to deterministic methods, MCRT was further adopted in an effort to more accurately capture the VLC channel characteristics. In [55], the wavelength dependency was explicitly taken into account in addition to the effect of mixed diffuse and specular reflections modelled with Phong's model. In this model, the surfaces are defined by three parameters for each wavelength: the reflection coefficient, the percentage of incident signal that is reflected diffusely, and the directivity of the specular component of the reflection (see eqn. (6) of [55]). The computational efficiency of ray tracing simulations is improved by first dividing the simulation environment into subcubes of equal size and second with parallelizing the simulation algorithm based on an equal and static distribution of the rays generated at the emitter among the available processors, i.e. assigning the rays to each processor by means of a uniform distribution.

While the Phong model is sufficiently accurate for most practical purposes, advanced models might be required to model surfaces with multiple reflection patterns. For this purpose, the bidirectional scatter distribution function (BSDFs) can be used, which basically includes the bidirectional reflectance distribution function (BRDF) and the bidirectional transmittance distribution function (BTDF) [60]. For most typical objects with opaque features, the BSDF model reduces to BRDF which assumes a solid, opaque sample surface and measures the reflectance of a target as a function of illumination geometry and viewing geometry [61]. Commonly used BRDF models are Lambertian, Phong, Retroreflective Phong, Blinn and Lafortune. The simplest BRDF model is obviously Lambertian [62] to model purely diffuse reflections, while the Phong BRDF [62], as discussed above, can take into account the effect of mixed diffuse and specular reflections. Retroreflective Phong BRDF [62] introduces a new reflection component in the direction of the incident ray (retroreflective specular component). Blinn BRDF [62] is another improvement over Phong's model and introduces a highly specular reflection component for incident angles away from the normal. Lafortune BRDF [62] is a composite model building on the previous models and defines four types of possible reflection components: the diffuse one (based on the Lambertian model) and three types of specular reflections (based on the Phong, Blinn and retroreflective models). To address the effect of adopted reflection models in ray tracing, the study in [56] investigated different BRDF models. It was shown that these models produce CIRs quite different from the basic Lambertian. These differences may imply variations of tens of MHz in bandwidth.

To decrease the computational complexity of ray tracing methods, a photon modelling method was proposed in [57]. Whereas the number of ray directions in traditional ray tracing techniques increases on each diffuse reflection, the number of directions in which each photon scatters is only one that is chosen to satisfy the surface property statistically. A comparison table of these works on VLC channel modelling can be found in table 1.

3. Site-specific channel modelling

In a series of papers [34,58,59], we have developed a site-specific channel modelling approach based on non-sequential ray tracing features of Zemax®. In this software, there are two modes of ray tracing. In sequential ray tracing [63], rays are traced through a sequence of surfaces, hitting each surface only once, while travelling from the transmitter to the receiver. This property makes sequential mode ideal for imaging systems. On the other hand, non-sequential ray tracing [63] allows rays to propagate through the environment in any order and allows rays to be scattered and reflected back to an object that they have already encountered. This property makes the non-sequential mode ideal for impulse response modelling which is also adopted in our study.

Our approach is able to obtain CIRs for various indoor environments with different shapes and sizes where any realistic light sources be easily integrated in the simulation environment. Furthermore, a large number of reflections (more than 10) can be easily handled for better accuracy including specular and mixed specular-diffuse reflections. Figure 5 provides an overall summary of major steps followed in the adopted channel modelling methodology. In the first step,

Table 1. Comparison table of works on indoor static VLC channel modelling.

	method	modelling of reflectance	number of reflections	other assumptions	observations and comments
[47]	recursive	fixed reflectance	third order	— purely Lambertian reflections — empty room — ideal Lambertian source	This study builds upon the recursive method proposed originally in [36] for IR channels. Spatial distributions of illuminance and RMS delay spread are presented for an empty room with a size of 5 m × 5 m × 3 m. Based on RMS values, it is concluded that the maximum bit rate that can be transmitted through the channel (without needing an equalizer) will be limited to 28 Mb s^{-1} for the simulation scenario under consideration. It should be noted that this study builds upon the simplifying assumptions of Lambertian source and purely diffuse reflections. More importantly, a fixed reflectance value is assumed ignoring the wavelength dependency in VL wavelengths.
[48]	recursive (iterative site-based)	averaged reflectance	fourth order	— purely Lambertian reflections — room with objects — ideal Lambertian source	This study builds upon the iterative recursive method proposed originally in [39] for IR channels. In an effort to decrease computation time, the first-order reflections are first obtained in this method, and then used to determine the higher-order reflections in an iterative manner. Simulations are carried out for two rooms with sizes of 5 m × 5 m × 3 m and 10 m × 10 m × 4 m. CIRs and frequency responses are presented for sample locations along with RMS delay spread. In addition, the so-called signal-to-ISI ratio is presented to determine the need for an equalizer. It should be noted that this study, similar to [47], builds on simplifying assumptions such as Lambertian source and purely diffuse reflections. In an effort to reflect the effect of wavelength dependency in channel modelling, the reflectance values are calculated as the average of wavelength-dependent coefficients over the VL band.

(*Continued*.)

Table 1. (*Continued*.)

	method	modelling of reflectance	number of reflections	other assumptions	observations and comments
[49]	recursive	wavelength dependent	third order	— purely Lambertian reflections — empty room — ideal Lambertian source	This study is based on the recursive algorithm of [36], but further takes into account the main differences between IR and VL channels. This is the first paper to account for the wavelength-dependent nature of reflectors in VLC channel modelling. Simulations are carried out for a room with size of 5 m $\times$ 5 m $\times$ 3 m and CIR is presented for plaster and plastic walls with notably different reflectance values. Comparisons are also made between IR and VLC channels and it is discussed that the total received power from reflected paths and the RMS delay spread of the VLC cases are smaller than those of the IR cases. It should be noted that, similar to [47,48], the work in [49] is also limited to the assumptions of only purely diffuse reflections and ideal Lambertian source which might not hold true for many practical cases.
[50]	recursive	fixed reflectance	third order	— purely Lambertian reflections — empty room — non-ideal Lambertian source	This study builds upon the recursive method of [36]. Simulations are carried out for a room with size of 5 m $\times$ 5 m $\times$ 3 m. The effects of two distinct non-Lambertian source radiation patterns on impulse and frequency responses, RMS delay spread, and path loss are quantified in comparison to ideal Lambertian radiation pattern. It should be noted that, similar to [47–49], the work in [50] is limited to the assumption of only purely diffuse reflections which cannot appropriately model the surfaces of most furniture. A fixed reflectance value is assumed ignoring the wavelength dependency in VL wavelengths.

(*Continued*.)

Table 1. (*Continued*.)

	method	modelling of reflectance	number of reflections	other assumptions	observations and comments
[51]	frequency-domain method	fixed reflectance	high order (>10)	— purely Lambertian reflections — empty room — ideal Lambertian source	This study develops a frequency-domain matrix formalism to describe the indoor channel for a room with Lambertian reflectors. Unlike time-domain approaches, this approach allows to take into account higher order reflections. Simulations are carried out for a room with size of 5 m × 5 m × 3 m and CIRs and frequency responses are presented for sample locations along with RMS delay spread. While high order reflections are considered for a realistic channel modelling in this study, there are some simplifying assumptions such as Lambertian source, purely diffuse reflections and fixed reflectance value.
[52]	geometric based	fixed reflectance	first order	— purely Lambertian reflections — empty room — ideal Lambertian source	This study proposes an analytical method with a relatively low computational complexity for calculating the non-LOS CIR. Simulations are carried out for a room with size of 5 m × 5 m × 3 m. The CIR obtained through this method is compared with that generated via ray tracing simulations. It is shown that the proposed method offers high accuracy for the first-order multipath components. It should be noted that this study builds on simplifying assumptions such as purely diffuse reflections, fixed reflectance value and ideal radiation pattern.
[53]	geometric based (FOV-GBSB)	averaged reflectance	first order	— purely Lambertian reflections — room with virtual scatterers — ideal Lambertian source	This study proposes a geometric-based method to simulate the VLC channels. Simulations are carried out for a room with size of 5 m × 5 m × 3 m and CIRs are presented along with angle of arrival (AoA) and channel gains. Similar to [48], this work uses an averaged reflectance value. It further assumes ideal Lambertian source and purely diffuse reflections.

(*Continued*.)

royalsocietypublishing.org/journal/rsta *Phil. Trans. R. Soc. A* **378**: 20190187

Table 1. (*Continued*.)

	method	modelling of reflectance	number of reflections	other assumptions	observations and comments
[54]	geometric based (RS-GBMB)	fixed reflectance	third order	— purely Lambertian reflections — room with virtual scatterers — ideal Lambertian source	This study proposes a geometry-based multiple bounce model for VLC channels. Simulations are carried out for room with size of 5 m $\times$ 5 m $\times$ 3 m and CIRs are presented for different number of reflections up to 3. It is shown that the LOS component carries a significant amount of power compared with the primary reflections (up to 3). This study builds on simplifying assumptions such as Lambertian source and purely diffuse reflections.
[55]	Monte Carlo ray tracing	wavelength dependent	high order (=10)	— diffuse, specular and mixed reflections — room with objects — ideal Lambertian source	This study builds upon the Monte Carlo ray tracing method proposed originally in [43] for IR channels. Simulations are carried out for a hexagonal room and CIR is presented for sample locations. It is shown that the computational efficiency can be improved by two optimization methods. The first one consists of dividing the geometry of the environment into cubic regions of equal size and the second one involves the parallelization of the simulation. Owing to low complexity implementation, higher order reflections are handled in this study for a more realistic channel modelling. Different types of reflections are also taken into account for precise characterization of surfaces. However, the ideal Lambertian model is still considered which might not be justified for most practical light sources.

(*Continued*.)

Table 1. (*Continued*.)

	method	modelling of reflectance	number of reflections	other assumptions	observations and comments
[56]	modified Monte Carlo ray tracing	fixed reflectance	third order	— diffuse, specular and mixed reflections — empty room — ideal Lambertian source	This study is an extension of the Monte Carlo ray tracing method of [43]. Each reflection of the rays is used to calculate an LOS contribution from the reflecting point to the receiver, thus using each ray multiple times instead of only once. This leads to a lower number of generated rays from the source to calculate an impulse response. Hence, this method is found to be faster compared to conventional ray tracing method. In addition, to address the effect of reflection models in ray tracing, the study investigates different BRDF models. Simulations are carried out for a room with size of 7.5 m $\times$ 5.5 m $\times$ 3.5 m and channel bandwidth is presented for different reflection models. The work however builds upon the simplifying assumptions of Lambertian source and a fixed reflectance value is assumed ignoring the wavelength dependency in VL wavelengths.
[57]	photon tracing	fixed reflectance	high order ($>$10)	— diffuse, specular and mixed reflections — room with objects — non-ideal Lambertian source	This study proposes a photon modelling method with a computation time that increases linearly with the number of reflections. This allows the consideration of higher order reflections. CIR is presented for a room with size of 5 m $\times$ 5 m $\times$ 3 m including furniture. A non-ideal Lambertian source is considered along with diffuse, specular and mixed reflections. However, similar to most of the above works, a fixed reflectance value is assumed ignoring the wavelength dependency in VL wavelengths.

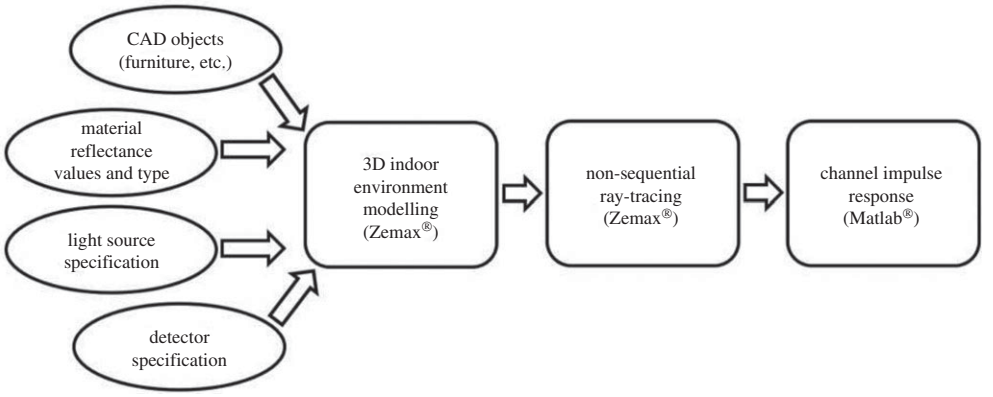

Figure 5. Main steps in site-specific channel modelling approach.

we create a three-dimensional (3D) simulation environment where we can specify the geometry of the indoor environment, the objects within, the reflection characteristics of the surface materials, and the specifications of the light sources and detectors. In the second step, we use non-sequential ray tracing to calculate the detected power and path lengths from source to detector for each ray. In the third step, we import these data to Matlab® and obtain the CIRs for the environment under consideration. Further details for each step are elaborated in the following.

(a) Modelling of the indoor environment

To model the simulation environment, we need to specify the dimensions and shape of the indoor environment, furniture and objects within, type of surface materials (coating), as well as the properties and locations of the transmitter (LED) and receiver (photodiode). The indoor environment (i.e. office room, living room, etc.) is created using Zemax® 'Part Designer', which is an interface that allows one to create and manipulate user-defined 3D geometries. The CAD objects can be imported in the software to model furniture and any other objects within the indoor environment. 'Table Coating Method' in the software further allows defining the wavelength-dependent reflectance of surface coating for each material.

Another important parameter in modelling of surface materials (walls, ceiling, furniture, etc.) is the type of reflections and opaqueness of object. As an example, figure 6 shows three different types where purely diffuse, specular and mixed reflections are observed. In our ray tracing approach, we can take into account the specific type of reflection by 'scatter fraction (SF)' parameter that determines the value of diffuse reflections in materials. This parameter changes between 0 and 1 such that zero indicates the purely specular reflections and unity indicates purely diffuse case. We adopt Phong BRDF model in our study to take into account the effect of mixed diffuse and specular reflections. In addition to realistic modelling of surface materials, our ray tracing approach also allows the use of realistic light sources. Several commercially available light sources are available in the Radiant Source Model (RSM) database [64]. The RSM file for a light source contains the measured radiant intensity (i.e. the radiant power of a source emitted in a certain direction) or luminous intensity (i.e. the luminous flux emitted by a source in a certain direction) of the source as a function of wavelength, position and angle. As such, this file can be accurately used to characterize the behaviour of the light source in both near- and far-fields.

In Zemax®, detectors can be modelled as planar surfaces, curved surfaces or 3D volumes which store the different data types such as radiant intensity and radiance (i.e. the intensity of optical radiation emitted or reflected from a certain location on an emitting or reflecting surface in a particular direction). Moreover, the data are available in radiometric and photometric units such as watts, lumens, lux, phot and footcandles. In our simulations, we use a rectangular surface with specified dimensions as a receiving element (i.e. 'Detector Rectangle' function in Zemax®).

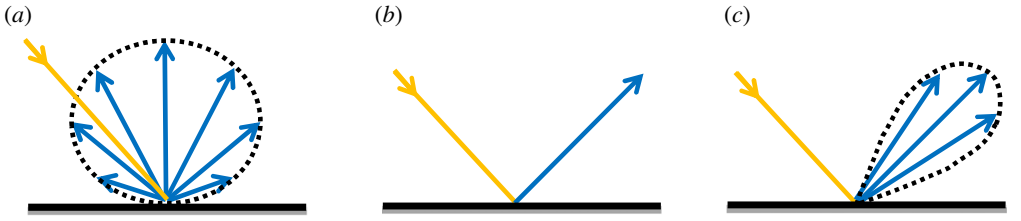

Figure 6. (*a*) Purely diffuse reflections, (*b*) specular reflections and (*c*) mixed reflections. (Online version in colour.)

(b) Non-sequential ray tracing

After we create the simulation environment, we use its non-sequential ray tracing feature to determine the CIR. In the ray tracing approach, rays are traced along a physically realizable path until they intercept an object. The LOS response is straightforward to obtain and depends upon the LOS distance. Besides the LOS component, there are a large number of reflections among ceiling, walls and floor, as well as any other objects within the environment. The way that non-sequential rays are traced depends on the source properties including polarization state, coherence length, initial phase, position and direction of rays of light emanating from non-sequential sources. The random ray tracing methods used in our approach are mainly based on Monte Carlo analysis [65] and Sobol sampling, the latter of which is used for speeding up ray tracing [66,67]. The main parameters in ray tracing are the number of rays and the number of reflections. The number of reflections our ray tracing approach is adjusted through 'Relative Minimum Intensity'. For example, if this parameter is set to 10^{-5}, the software runs until the ratio of the intensity of last segment with respect to the first segment becomes 10^{-5}.

(c) Channel impulse response construction and characterization

From non-sequential ray tracing, we obtain the detected power and path lengths from source to detector for each ray. We import this file to Matlab®, and using this information we can construct the CIR as

$$h(t) = \sum_{j=1}^{N_r} P_j \delta(t - \tau_j), \tag{3.1}$$

where P_j is the optical power of the jth ray, τ_j is the propagation time of the jth ray, $\delta(t)$ is the Dirac delta function and N_r is the number of rays received at the detector.

Once we obtain CIRs, we can calculate fundamental channel parameters such as DC gain and delay spread. Channel DC gain is calculated as

$$H_0 = \int_0^\infty h(t) \mathrm{d}t. \tag{3.2}$$

Based on (3.2), the path loss can be calculated as [68]

$$\mathrm{PL} = -10 \log_{10} H_0. \tag{3.3}$$

The time dispersion parameters of channel, RMS delay spread and mean excess delay are, respectively, given by [58]

$$\tau_{\mathrm{RMS}} = \sqrt{\int_0^\infty (t - \tau_0)^2 h(t)\, \mathrm{d}t \Big/ \int_0^\infty h(t)\, \mathrm{d}t}. \tag{3.4}$$

and

$$\tau_0 = \int_0^\infty t h(t) \mathrm{d}t \Big/ \int_0^\infty h(t) \mathrm{d}t\ . \tag{3.5}$$

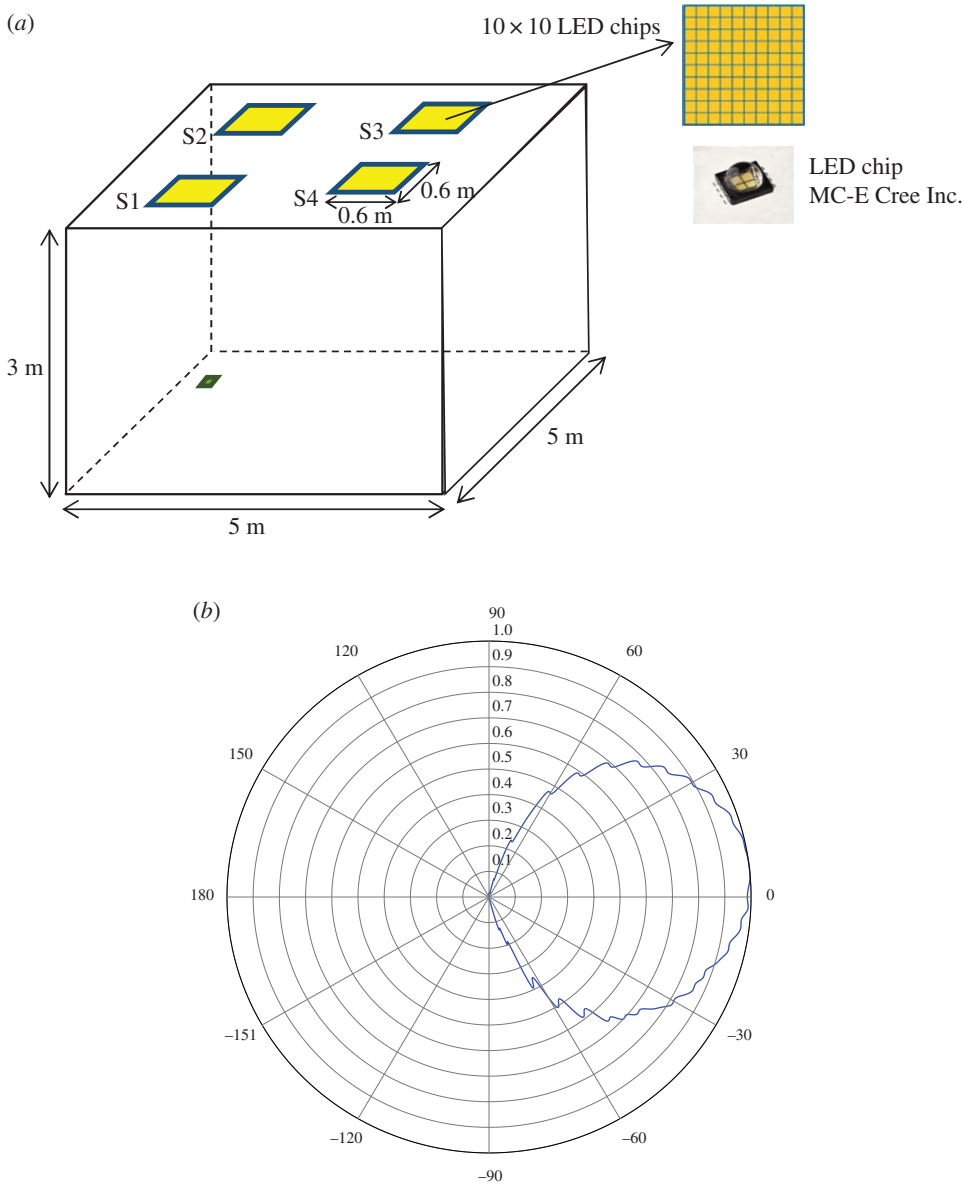

Figure 7. (*a*) Three-dimensional environment and (*b*) emission pattern of source. (Online version in colour.)

(d) Numerical results

In this section, we consider an empty room size of 5 m × 5 m × 3 m where four LED luminaires are located on the ceiling and the detector is located at the corner of the floor as illustrated in figure 7*a* [58]. An LED luminaire consists of 100 LED chips and each chip radiates 0.45 W with a full angle of half power of 120°. The FOV and area of the detector are 85° and 1 cm^2, respectively. We use Cree Xlamp® MC-E White LED (figure 7*b*) which has nearly ideal Lambertian pattern [58]. The simulation parameters are summarized in table 2.

In figure 8, only LOS is considered, i.e. $k = 0$. It is observed that three peaks exist in CIR which are related to four LED lightings. The largest one corresponds to the nearest LED (S2). The second peak is the joint contribution of two LEDs (S1 and S3) which are at the same distance from the PD. The third peak is related to the further LED (S4).

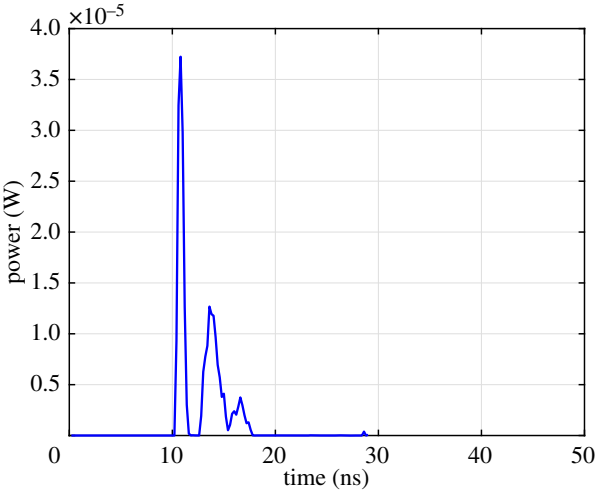

Figure 8. CIR for $k = 0$ (only LOS is considered). (Online version in colour.)

Table 2. Simulation parameters.

size of room (m)	$5 \times 5 \times 3$
time resolution (Δt)	0.2 (ns)
number of lighting	4
number of chips per each lighting	100
power of each chip	0.45 (W)
lighting positions (m)	(1.5,1.5,3), (1.5,3.5,3) 3.5,1.5,3), (3.5,3.5,3)
PD position (m)	(0.5,1,0)
full angle of half power of lighting	120°
FOV of PD	85°
area of PD	1 (cm^2)
materials	purely diffuse reflections

In figure 9, we investigate the effect of first-order reflections. Figure 9*a* presents the first-order reflection terms, while figure 9*b* is the aggregated CIR where both LOS and first-order reflections are considered simultaneously. It is observed that first-order reflections contribute some non-negligible increase in both amplitude and delay spread. Mathematically speaking, the channel DC gain increases from 4.82×10^{-5} to 6.03×10^{-5} and RMS delay spread increases from 2.10 to 3.33 ns.

In figure 10, we investigate the effect of second-order reflections. It is observed that second-order reflections make a very slight increase in the amplitudes but effectively increases the delay spread of CIR. Specifically, the channel DC gain increases from 6.03×10^{-5} to 7.06×10^{-5}, while RMS delay spread increases from 3.33 to 6.60 ns.

In figure 11, we present the CIR where we assume $k = 3$ reflections. As a benchmark, we include the CIR of [49] obtained through the recursive method. Since the results in [49] are also obtained for $k = 3$ reflections, this gives an opportunity to make a one-to-one comparison. It is observed from figure 11 that two CIRs are almost identical confirming the accuracy of our

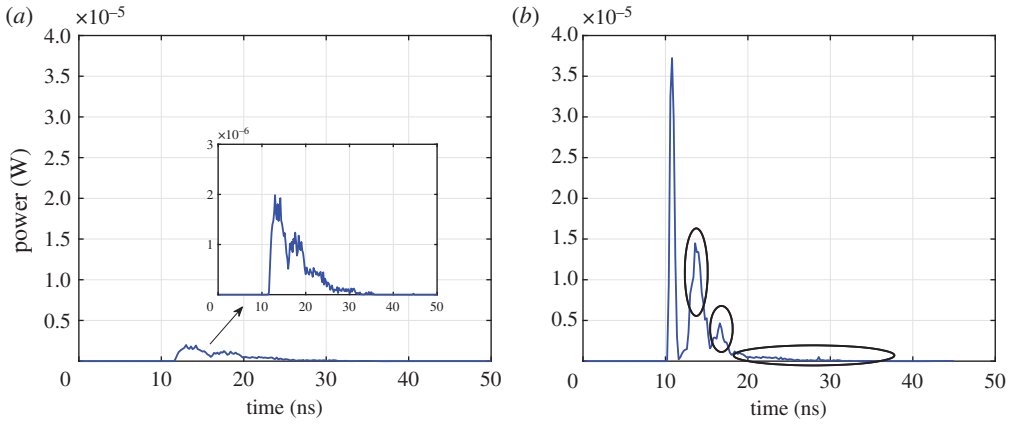

Figure 9. (*a*) CIR for first-order reflections and (*b*) CIR for $k = 1$ (i.e. LOS and first-order reflections). (Online version in colour.)

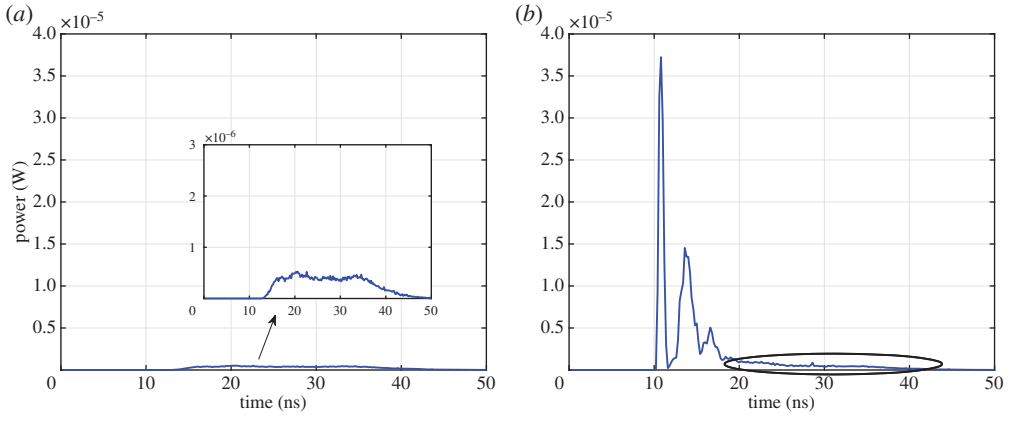

Figure 10. (*a*) CIR for second-order reflections and (*b*) CIR for $k = 2$ (i.e. LOS, first- and second-order reflections). (Online version in colour.)

approach. Some small differences between the tails of two CIRs are observed. This is due to the fact that our light source is a commercial light source and does not behave exactly as a Lambertian source (figure 7*b*) unlike the ideal source assumed in [49].

In an effort to have a better understanding of the impact of higher order reflections, figure 12 presents the channel DC gain and RMS delay spread with respect to reflection numbers. It is observed that there is no notable change for values larger than $k = 4$ in an empty room under consideration.

In figure 13, we investigate the effect of reflection types. Most existing works [47–54] build upon the assumption of purely diffuse reflections. In contrast, our approach can handle other type of reflections. In the following, we assume mixed reflections (figure 13*a*) and mostly specular reflections (figure 13*b*) where SF is set to 0.5 and 0.2, respectively. It is observed from figure 13*a*,*b* that the presence of specular components creates fluctuations in CIR and results in deviations from the purely diffuse case. This is particularly evident in figure 13*b* where mostly specular case is considered. In diffuse case, when one ray reflects from the surface, the power of ray decays by reflection coefficient and that power is divided among scattering rays. On the other hand, in specular case, the power of ray just decays by reflection coefficient and there is no division of power among scattering rays. By considering specular components for materials, the power of rays decays slowly which results in fluctuations of CIR.

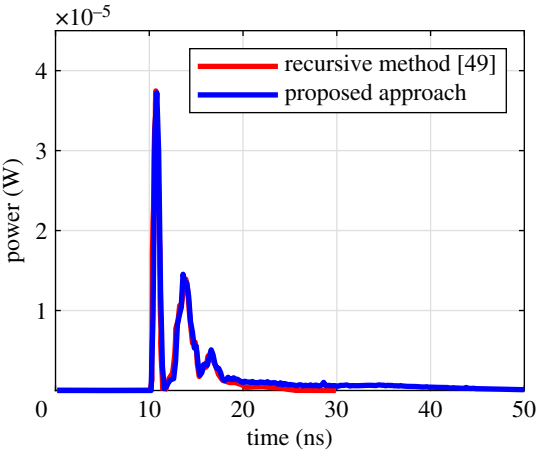

Figure 11. CIR for $k = 3$ and comparison with recursive method in [49] for the same number of reflections. (Online version in colour.)

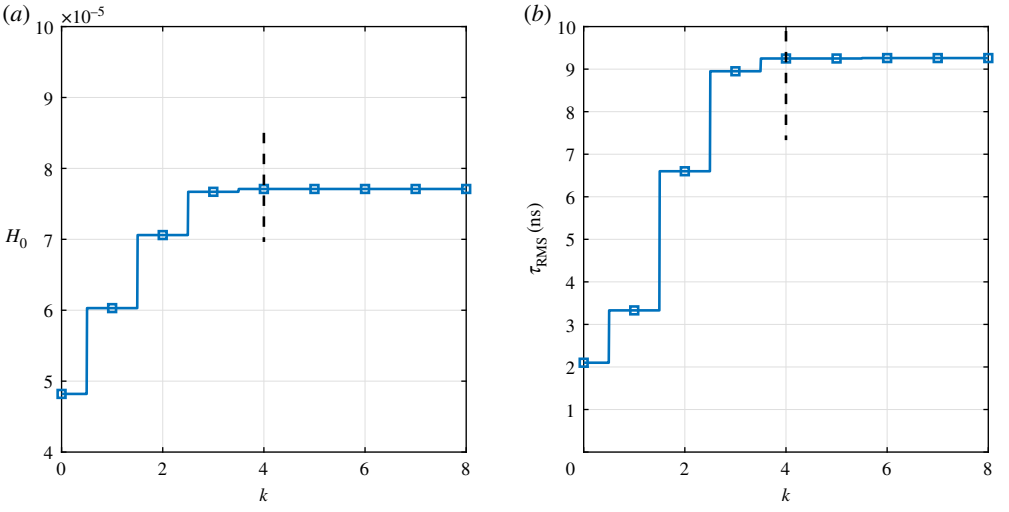

Figure 12. (*a*) Channel DC gain and (*b*) RMS delay spread versus number of reflections assuming diffuse reflections. (Online version in colour.)

Finally, figure 14 presents the DC gain and RMS delay spread with respect to the number of reflections for mixed and mostly specular reflection cases. It is observed from figure 14 that, in the mixed case, the value of channel DC gain saturates after three reflections while the saturation of RMS delay spread occurs after four reflections. In the mostly specular case, there is no significant change in channel DC gain after eight reflections while RMS delay spread becomes constant after nine reflections.

4. IEEE reference channel models

In line with the growing attention on VLC, the IEEE has initiated relevant standardization activities. In December 2014, the Task Group 802.15.7r1 (later named 802.15.m) 'Short Range Optical Wireless Communications' was formed. This task group was responsible for the

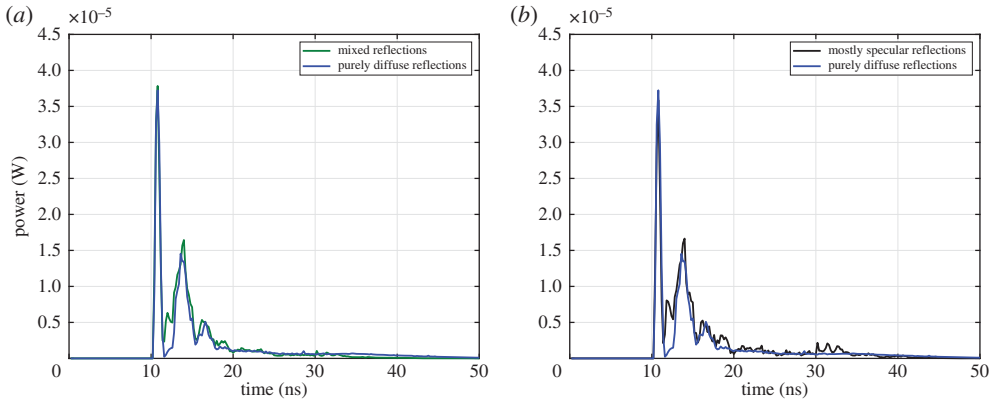

Figure 13. Comparison of CIRs (*a*) purely diffuse versus mixed and (*b*) purely diffuse versus mostly specular. (Online version in colour.)

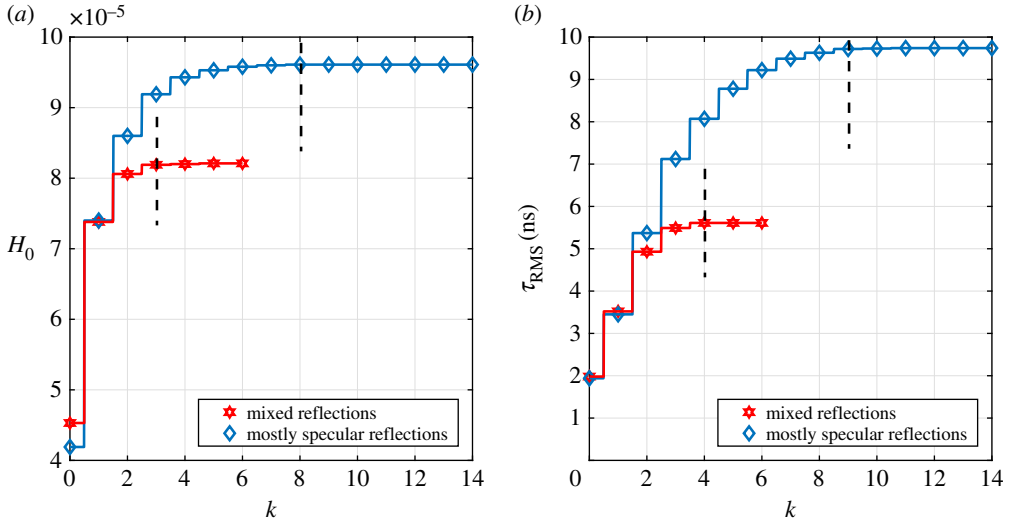

Figure 14. (*a*) Channel DC gain and (*b*) RMS delay spread versus number of reflections assuming mixed reflections and mostly specular reflections. (Online version in colour.)

development of both optical camera communication (OCC) and high-speed VLC where smartphone cameras and photodetectors are, respectively, used as receivers. In March 2017, a spin-off group dedicated on high-speed VLC was established and named as IEEE 802.15.13.

In standardization works, to make a fair performance comparison between various system proposals, a critical issue is to establish reference channel models. Based on the methodology described in §3, CIRs were obtained for typical indoor environments including home, office and manufacturing cell and these were endorsed by the IEEE as VLC reference channel models [69,70]. The four scenarios under consideration include workplace (open office floor and cubicles), office room with secondary light, living room and manufacturing cell. In the following, we describe each of these scenarios, present associated CIRs and discuss the relevant channel parameters.

(a) Scenario descriptions

In the first reference scenario, two workplaces are considered where six office desks with working personnel are located. Both workplaces have identical sizes with dimensions of 14 m × 14 m × 3 m.

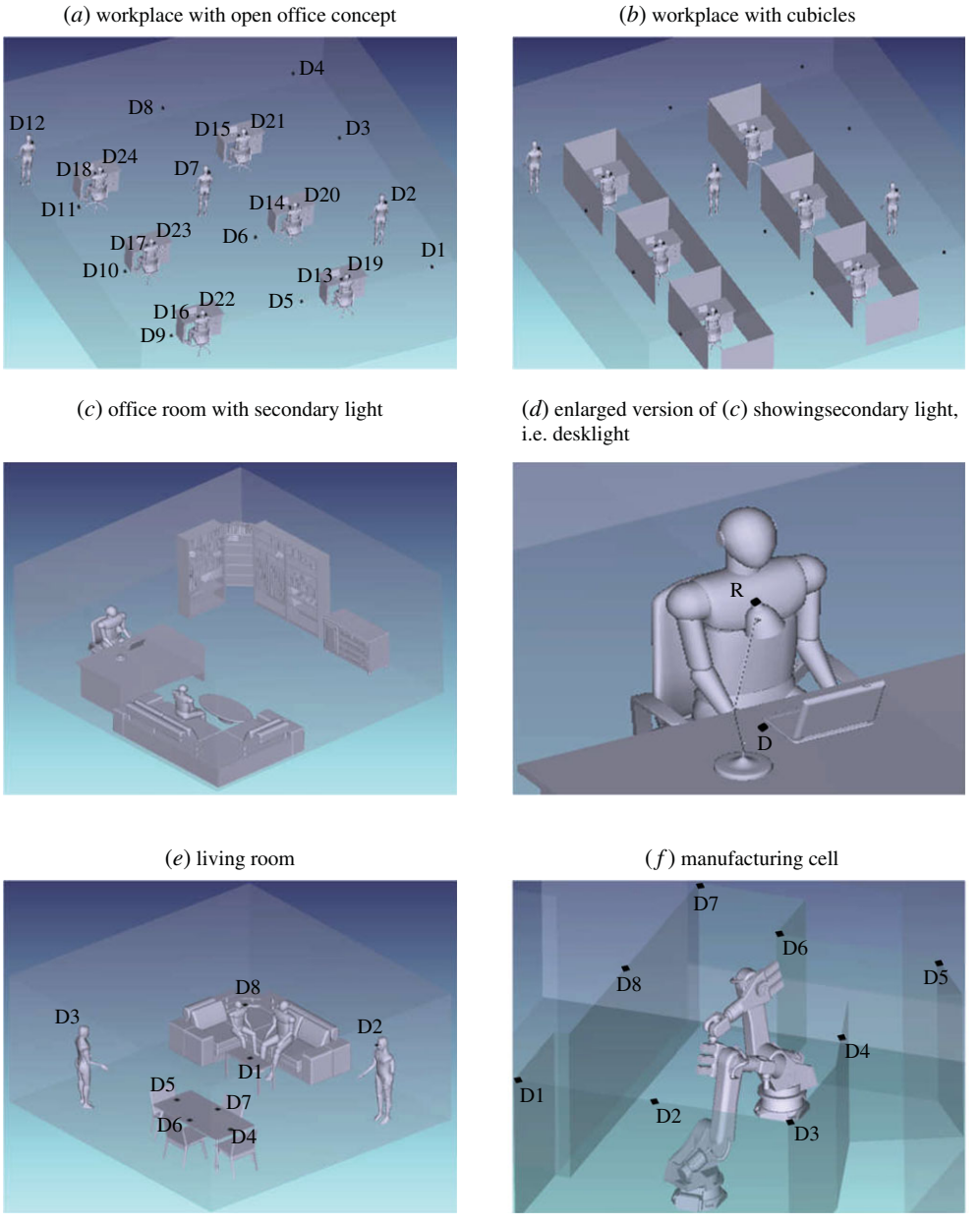

Figure 15. Indoor reference scenarios. (Online version in colour.)

The first one has an open office layout (figure 15*a*) while the second one (figure 15*b*) has cubicles. Thirty-two luminaires are uniformly located in a rectangular grid at the ceiling. The luminaires used in simulations are commercially available (Cree® LR24-38SKA35). They have a non-ideal Lambertian pattern, a semi-angle of half power of 40° and luminous efficacy (i.e. the ratio of luminous flux to optical power) of 73 lumens per watt. The illumination levels are provided in figure 16*a*. It can be readily checked that the minimum, maximum and average values of illumination are 278 lx, 712 lx and 533 lx, respectively. It can be noted that the average value satisfies the required typical illumination level of 500 lx for workplaces [71].

In the second scenario, an office room with a size of 5 m × 5 m × 3 m is considered (figure 15*c*). It is assumed that there are two light sources. One of them is the main ceiling light, while the other

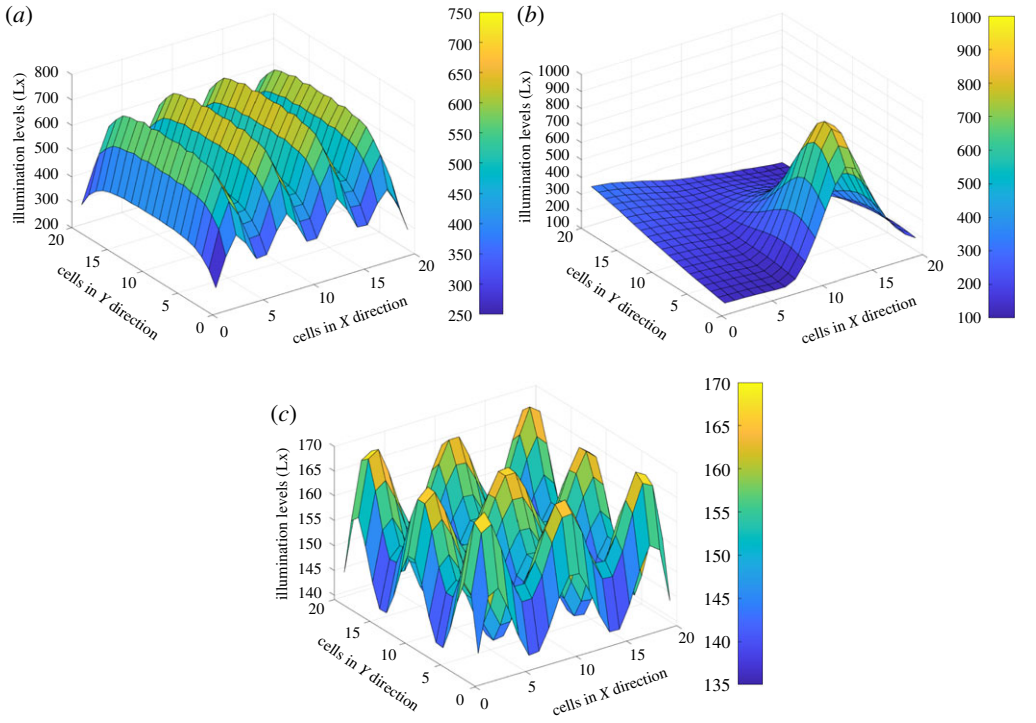

Figure 16. Illumination levels for (*a*) workplace, (*b*) office room with secondary light and (*c*) living room. (Online version in colour.)

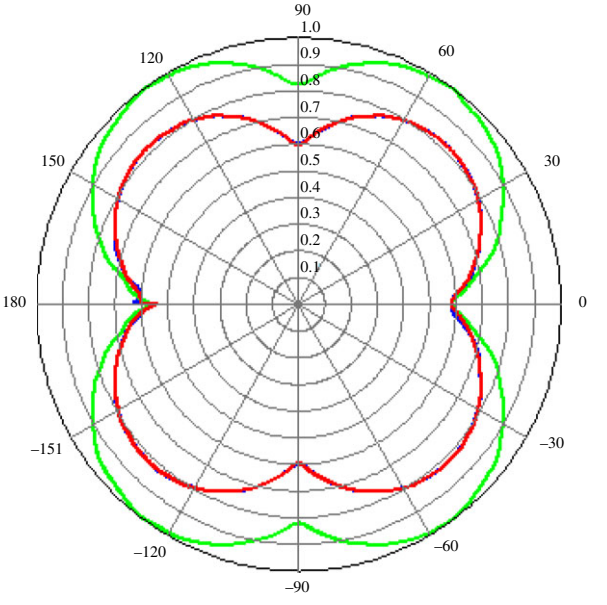

Figure 17. Emission pattern of cubic transmitter with six LEDs in manufacturing cell scenario assuming scanning angles of 45° and 90°, respectively, indicated by green and red colour. (Online version in colour.)

one is a desk light. Such a scenario is particularly useful to evaluate the performance of relay-assisted (cooperative) VLC systems [25] where the ceiling light acts as the source and the desk light serves as the relay (figure 15*d*). The destination receiver is on the desk next to the laptop. This might, for example, take the form of a USB device connected to laptop. The relay receiver is on the top of desk light with 45° rotation towards the source on the ceiling. As illustrated in figure 16*b*, the minimum, maximum and average values of illumination are calculated as 119 lx, 902 lx and 270 lx, respectively. The average value satisfies the required typical illumination level of 250 lx for easy office work [71].

In the third scenario, a living room of size 6 m × 6 m × 3 m is considered (figure 15*e*). Four persons are present in the room: two sitting on the couch with other two standing. Nine luminaires (Cree® CR6-800 L) are uniformly located in a rectangular grid at the ceiling. They have a semi-angle of half power of 40° and 67 lumens per watt efficacy. The minimum, maximum and average values of illumination are 139 lx, 169 lx and 153 lx, respectively (figure 16*c*). It can be noted that this average illumination level satisfies typical illumination level requirement of 150 lx for living rooms [71].

In the fourth scenario, a manufacturing cell of size 8.03 m × 9.45 m × 6.8 m is considered (figure 15*f*). The other details of manufacturing cell can be found in [69]. Six LED transmitters are located at the head of the robotic arm which has a form of cube. Each face of the cube is equipped with one transmitter ensuring 360° coverage. The LEDs are commercially available (Cree® MC-E) with non-ideal Lambertian pattern and a semi-angle of half power of 60°. The FOV and the area of the detector are 35° and 1 cm^2, respectively. The illumination level is not of concern for this type of application. It should, however, be noted that the cubic transmitter design provides an omni-directional coverage as illustrated in figure 17.

(b) Channel impulse responses for reference scenarios

In the first scenario, 24 different test points are selected (denoted by black circles in figure 15*a*) and the corresponding CIRs can be found in [69]. Table 3 summarizes the channel DC gains and RMS delay spreads for these CIRs. With respect to an open office, channel DC gains in the office with cubicles decrease. Specifically, a 7.6% decrease in the average value of DC gains over 24 test points is observed. This decrease is a result of the presence of cubicles. The rays within cubicles hit the cubicle walls and decay more rapidly than those rays in the open office. Since the rays cannot pass through cubicle walls (i.e. the cubicle walls are sufficiently thick) and, delay spread values in the office with cubicles are also smaller, i.e. 16.9% decrease.

In the second scenario, two test points are considered which correspond to relay and destination. The CIRs are provided in [69] and table 4 summarizes the main channel characteristics. It can be observed that the relay to destination (R → D) channel is stronger than the source to destination (S → D) channel since the relay transmitter is closer to the destination and therefore experiences smaller path loss. It is also observed that the S → D channel has more scattering components inducing a larger delay spread. Since the distance between source and destination is larger than the distance between relay and destination, the rays coming out from the source hit more surfaces (i.e. wall, floor and objects inside the room) and result in more scattering.

In the third scenario, eight different test points are selected. The corresponding CIRs can be found in [69] and channel parameters are summarized in table 5. It is observed that the channel DC gains in the living room are smaller than those observed in the workplace since the room dimensions are now smaller.

In the fourth scenario, eight different test points (denoted by Dn , $n = 1, \ldots, 8$ in figure 15*f*) are considered on top of the cell boundaries and relevant channel parameters are provided in table 6. It is observed that the amplitude of D4 is much larger than that of D7 because this detector is closer to the set of transmitters. Since D7 is located at the corner of the cell boundary, it receives more scattering from boundaries. On the other hand, the RMS delay spread of D7 is much larger than that of D4.

Table 3. Channel parameters for workplace.

	open office		office with cubicles	
	τ_{RMS} (ns)	H_0	τ_{RMS} (ns)	H_0
D1	13.30	1.00×10^{-3}	11.26	9.55×10^{-4}
D2	17.04	5.26×10^{-4}	15.38	5.03×10^{-4}
D3	17.15	9.22×10^{-4}	14.41	8.85×10^{-4}
D4	14.98	1.26×10^{-3}	11.98	1.22×10^{-3}
D5	14.73	9.06×10^{-4}	12.91	8.32×10^{-4}
D6	15.38	9.96×10^{-4}	14.04	9.54×10^{-4}
D7	18.80	5.19×10^{-4}	17.08	4.77×10^{-4}
D8	15.95	1.06×10^{-3}	14.75	1.06×10^{-3}
D9	13.99	9.29×10^{-4}	11.39	8.87×10^{-4}
D10	13.84	1.20×10^{-3}	12.47	1.14×10^{-3}
D11	17.24	9.21×10^{-4}	14.60	9.19×10^{-4}
D12	17.85	7.08×10^{-4}	15.90	6.92×10^{-4}
D13	13.15	8.74×10^{-4}	10.02	8.00×10^{-4}
D14	13.97	8.45×10^{-4}	11.88	5.33×10^{-4}
D15	15.79	5.16×10^{-4}	12.39	4.91×10^{-4}
D16	12.39	9.03×10^{-4}	9.44	8.89×10^{-4}
D17	16.23	4.96×10^{-4}	12.60	4.12×10^{-4}
D18	14.63	7.41×10^{-4}	10.71	6.78×10^{-4}
D19	12.99	1.05×10^{-3}	10.88	7.51×10^{-4}
D20	13.65	7.09×10^{-4}	10.71	6.67×10^{-4}
D21	15.41	6.57×10^{-4}	10.74	6.45×10^{-4}
D22	16.15	5.15×10^{-4}	13.62	4.73×10^{-4}
D23	16.11	5.84×10^{-4}	13.24	5.54×10^{-4}
D24	15.95	6.75×10^{-4}	12.15	6.24×10^{-4}
average	15.27	8.13×10^{-4}	12.68	7.51×10^{-4}

Table 4. Channel parameters for office room with secondary light.

	τ_{RMS} (ns)	H_0
R $\longrightarrow$ D	1.37	1.30×10^{-4}
S $\longrightarrow$ D	7.76	2.81×10^{-6}
S $\longrightarrow$ R	8.32	7.13×10^{-6}

As a final remark, we need to point to out that IR sources are typically used in the uplink, e.g. current product offerings from different companies [72,73]. In an effort to give an idea about the uplink channels, we further provide CIRs for the uplink assuming IR light sources in the second scenario. We assume that each USB hub of source terminal (in the form of laptop) is equipped with four IR LEDs (figure 18*b*). The separation between adjacent IR LEDs is taken as 5 cm. The distance between adjacent USB hubs is 12.5 cm. The IR LED has a full angle of half power of 120°. We equip

Table 5. Channel parameters for living room.

	τ_{RMS} (ns)	H_0
D1	9.64	1.82×10^{-4}
D2	8.30	3.31×10^{-4}
D3	7.19	3.26×10^{-4}
D4	9.90	2.44×10^{-4}
D5	10.16	2.58×10^{-4}
D6	9.62	2.74×10^{-4}
D7	10.30	2.31×10^{-4}
D8	8.83	2.47×10^{-4}
average	9.24	2.61×10^{-4}

Table 6. Channel parameters for manufacturing cell.

	τ_{RMS} (ns)	H_0
D1	13.48	1.16×10^{-6}
D2	13.33	2.99×10^{-6}
D3	11.68	4.46×10^{-6}
D4	6.79	2.15×10^{-5}
D5	14.36	1.94×10^{-6}
D6	12.54	1.22×10^{-6}
D7	13.66	5.69×10^{-7}
D8	11.00	4.67×10^{-6}

each of 16 luminaires on the ceiling with one PD (figure 18*a*). The FOV and area of PD are 85° and 1 cm^2, respectively. The corresponding CIRs are provided in [74]. Table 7 summarizes the main channel characteristics. It is observed that DC gains and RMS delay spreads of VL channels are smaller than those in IR channels. This is mainly due to the reason that reflectivity values in the IR band are larger than those in the VL band.

5. Mobile visible light communication channels

As discussed in the previous sections, most works on VLC channel modelling focus on scenarios where transmitter and receiver are located at fixed points. In practice, user mobility should be taken into account that will have important implications for system design issues such as handover. There are only sporadic works which consider mobility in VLC channel modelling [75–78]. In [78], the shadowing effect caused by the human body was considered for VLC channel characteristics. This, however, builds on some simplifying assumptions such as ideal Lambertian source and purely diffuse reflections. Another simplifying assumption in [75,76,78] was fixed reflectance values for surface materials (i.e. wall, floor, etc.). In [68], we adopted our ray tracing channel modelling approach in [58] to obtain the CIRs over different user movement trajectories. The comparison of these works is presented in table 8.

The work in [68] builds upon the assumption of a single PD and a specific orientation between transmitter and receiver. In practice, to ensure an omni-directional coverage, the mobile receiver will be likely equipped with multiple PDs. To address such issues of practical importance, we investigate the effect of photodetector location/orientation within this section. We consider a

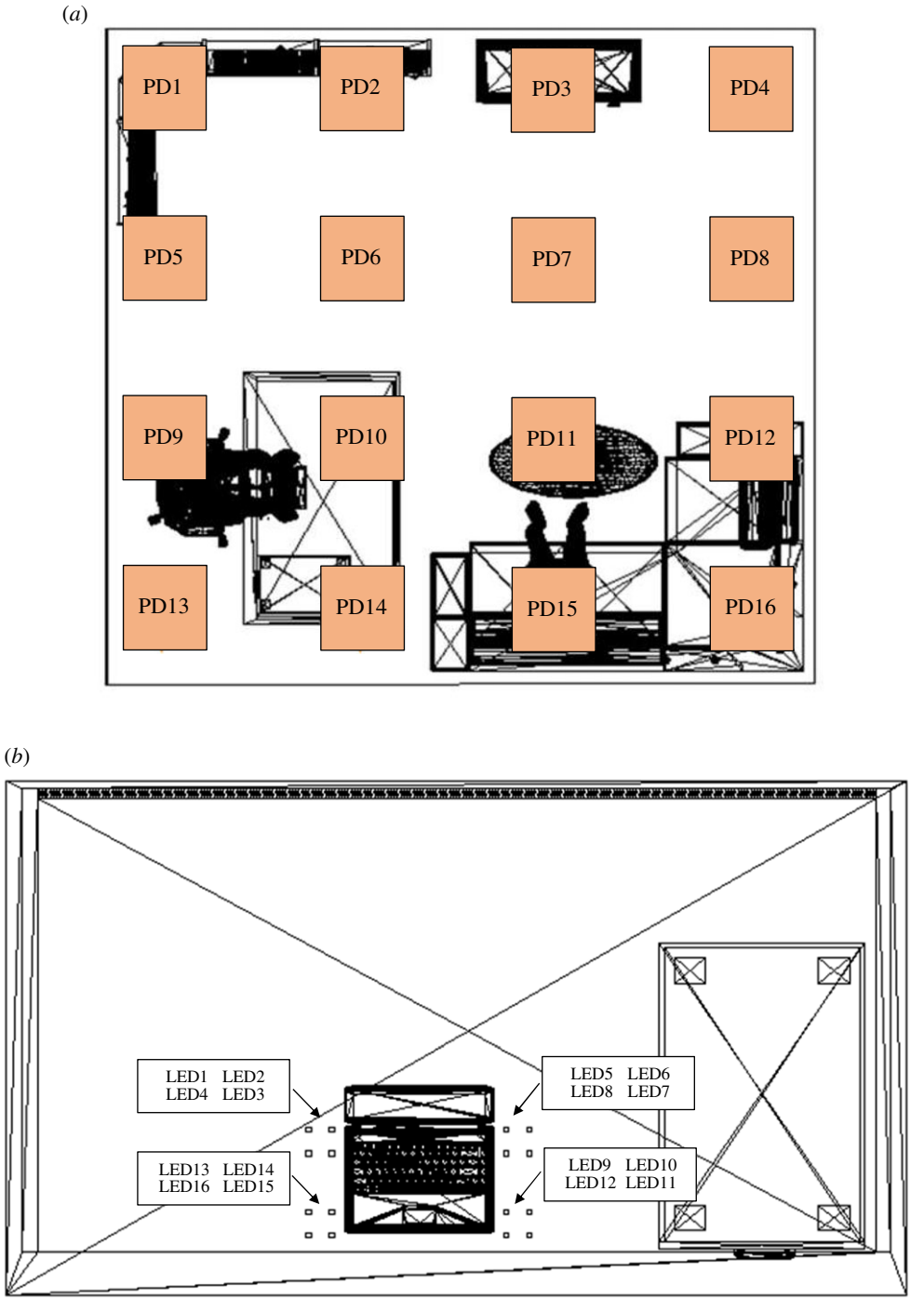

Figure 18. (*a*) Arrangement of PDs on the ceiling and (*b*) top view of the desk with laptop and IR LEDs. (Online version in colour.)

mobile receiver terminal in the form of a cell phone. Seven possible locations are considered for the photodetector. Five of these are on the top edge and two of them are on the top round corners of the device. For each possible location of a photodetector, we obtain CIRs and corresponding

Table 7. Channel parameters of uplink IR channels as seen by PD1.

	τ_{RMS} (ns)	H_0
LED1	8.69	1.56×10^{-6}
LED2	8.48	1.49×10^{-6}
LED3	8.29	1.32×10^{-6}
LED4	8.28	1.76×10^{-6}
LED5	8.90	1.21×10^{-6}
LED6	9.17	1.06×10^{-6}
LED7	8.62	1.26×10^{-6}
LED8	8.28	1.23×10^{-6}
LED9	8.89	1.05×10^{-6}
LED10	8.93	9.69×10^{-7}
LED11	8.82	1.14×10^{-6}
LED12	9.12	1.02×10^{-6}
LED13	8.04	1.67×10^{-6}
LED14	8.83	1.12×10^{-6}
LED15	8.54	1.23×10^{-6}
LED16	8.82	1.52×10^{-6}

path loss. To further demonstrate the effects of user location, we present the spatial distribution of channel gain within the room.

We consider a room with a size of 6 m × 6 m × 3 m as illustrated in figure 19 with plaster ceiling/walls and a pinewood floor. We assume nine luminaires on the ceiling with equidistance spacing. These are commercially available LEDs (Cree® CR6-800 L) with 40° semi-angle of half power. The optical power for each luminaire is 11 W. This yields an average illumination level of 153 lx which satisfies typical illumination levels for home environment [71].

We consider a user with a height of 1.8 m and model the human body as a CAD object (https://grabcad.com/library/28376) (figure 20*a*) with absorbing property [77]. The cell phone has a size of 5.5 cm × 10.5 cm × 0.5 cm and is equipped with a single photodetector. The user holds the phone in his hand next to his ear with 45° rotation upward and at a height of 1.65 m. We consider seven possible locations for the photodetectors denoted as Dn , $n = 1, \ldots, 7$ (figure 20*b*). D1, . . . , D5 are placed on the top edge of the cell phone, while D6 and D7 are placed on the top two round corners of the cell phone. The FOV and the area of each detector are 85° and 1 cm^2, respectively.

To further investigate the effects of user locations, we consider 100 cells with equidistant spacing of 0.6 m in x and y directions. The user is assumed to be standing in the middle of the cell where his/her body is perpendicular to the floor and he/she always stands parallel to y direction. As case study, we consider 10 example locations for the user denoted as $P_{1,3}$, $P_{2,8}$, $P_{3,1}$, $P_{4,4}$, $P_{5,9}$, $P_{6,5}$, $P_{7,2}$, $P_{8,7}$, $P_{9,10}$ and $P_{10,6}$ (i.e. indicated with yellow squares in figure 19). For the sake of simplicity and without loss of generality, the effective channel responses as seen by photodetector D5 are illustrated in figure 21 assuming cut-off frequency of $f_{cut-off} = 20$ MHz [79]. It is observed that the low-pass characteristics of LED result in some attenuation towards higher frequencies. It is also observed that in the effective channel responses of $P_{1,3}$, $P_{10,6}$ and $P_{9,10}$ frequency selectivity is more pronounced. It is a result of the fact that these locations are close to the walls (figure 19) and, therefore, more reflected rays are received. It might be also interesting to observe somehow different channel characteristics observed for $P_{1,3}$ and $P_{3,1}$, although these locations are symmetrical in space. This is mainly due to the position of the user who stands

Table 8. Comparison table of works on indoor mobile VLC channel modelling.

	method	modelling of reflectance	number of reflections	other assumptions	observations and comments
[75,76]	recursive	fixed reflectance	first order	— purely Lambertian — empty room — mock-up human body (i.e. cylindrical object) — multiple luminaires — ideal Lambertian source	These studies ([76] is a journal version of [75]) build upon the recursive method of [36]. Simulations are carried out for room with size of 5 m × 5 m × 3 m assuming the mean density of pedestrians in the range of 0.01–0.1 m^{-2} with uniformly distributed velocity (0–4 km h^{-1}), uniformly distributed orientation (0–2π rad) and walking time 5 s. As performance metrics, outage area per service area versus data rate, outage call duration rate versus mean density of pedestrians and blocking rate versus height of human body are presented. It is discussed that the selection of the optimal number of the LED lighting can mitigate the shadowing. This study builds on a number of simplifying assumptions such as Lambertian source, purely diffuse reflections and ignores the wavelength dependency of reflectance value in VL wavelengths.
[77]	Monte Carlo ray tracing	wavelength dependent	high order (>4)	— purely Lambertian — empty room — mock-up human body (i.e. cuboid object) — single luminaire — ideal Lambertian source	This study builds upon the Monte Carlo ray tracing method of [43]. Simulations are carried out for a room with size of 8 m × 10 m × 2.5 m assuming two different people with height of 150 and 180 cm. They move between transmitter and receiver with a step distance of 40 cm. Path loss and RMS delay spread are presented. It is shown that human shadowing has an adverse effect on the VLC system under LOS scenario, and by changing the relative angle, it is possible to mitigate the human shadowing effect. As for the NLOS scenario, the further away the receiver is from the LED, the more sensitive to human shadowing the VLC system will be. It should be noted that this study builds on some simplifying assumptions similar to [75,76]. In addition, a simplified cylindrical object is used to model the human body which cannot accurately capture the effect of the user body.
[78]	recursive	fixed reflectance	first order	— purely Lambertian — room with furniture — multiple luminaires — ideal Lambertian source	This study builds upon the recursive method of [36]. Simulations are carried out for three room types, i.e. corridor, office and hall, with sizes of 20 m × 20 m × 3 m, 6 m × 7 m × 3 m and 12 m × 8 m × 3 m, respectively. The people are randomly distributed within the room where the number of people is chosen to follow approximately the same people density for different room types, i.e. 0.16 people m^{-2} and 0.17 people m^{-2}. The position of each person is chosen to be different and people are randomly moved for 30 s. The CDF of received power and RMS delay spread are presented along with the spatial distribution of received power. It is shown that the PDF of the normalized received power has a match to Rayleigh distribution. Similar to [75–77], this study builds on some simplifying assumptions on reflection type and source pattern.

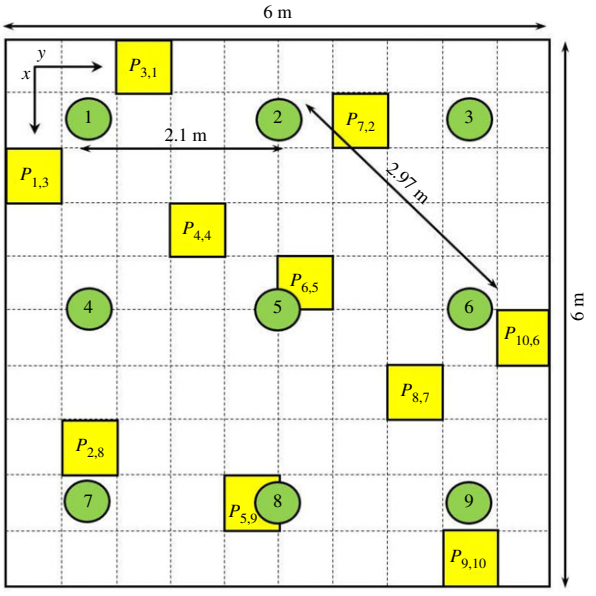

Figure 19. Room under consideration with green circles denoting luminaires and yellow squares denoting the example locations of the user. (Online version in colour.)

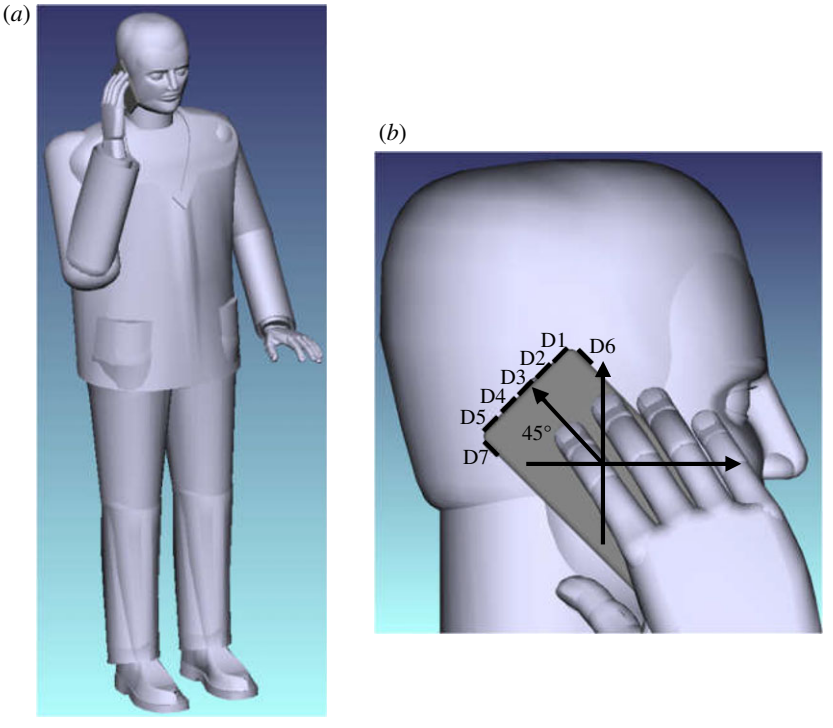

Figure 20. (*a*) Human model and (*b*) location and rotation of PDs on the cell phone. (Online version in colour.)

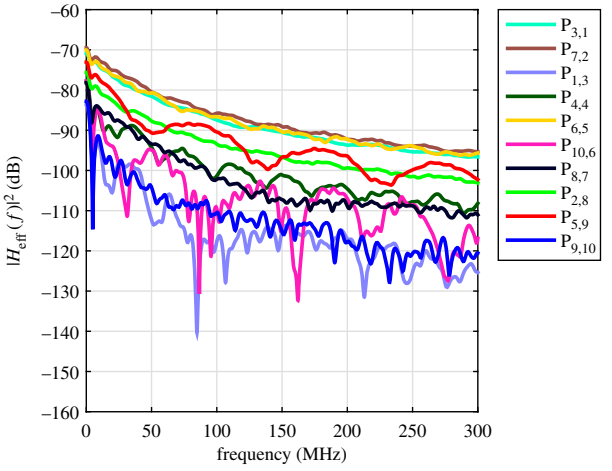

Figure 21. Effective channel responses as seen by photodetector D5 for the sample locations of the user. (Online version in colour.)

Table 9. Channel parameters for scenario under consideration.

	τ_{RMS} (ns)	H_0
D1	13.92	0.60×10^{-5}
D2	14.10	0.60×10^{-5}
D3	14.07	0.63×10^{-5}
D4	14.09	0.69×10^{-5}
D5	14.10	0.72×10^{-5}
D6	14.06	0.62×10^{-5}
D7	13.22	0.30×10^{-5}

parallel to the y direction and holds the cell phone in his right hand. When the user stands in $P_{3,1}$, the received signal is mainly dominated by the LOS component from luminaire 1. On the other hand, there is no LOS signal in $P_{1,3}$ and the received signal mainly depends on reflected signals.

In figure 22, we illustrate the spatial distribution of channel gain as seen by the individual photodetectors Dn , $n = 1, \ldots, 7$. It is observed that as the user moves within the room, the spatial distributions of channel gain seen by photodetectors D1, ... , D6 follow the sinusoidal pattern in x and y directions. When the user approaches to a luminaire, the signal strength increases. The maximum signal strength (i.e. maximum value of channel gain) occurs when the user is right under the luminaire. When the user walks away, the signal strength decreases. On the other hand, the spatial distribution of channel gain seen by photodetector D7 is almost flat (i.e. the same channel gain for all cells). This is a result of the fact that this detector is oriented towards the floor and the detector only captures reflected rays, i.e. there is not LOS component.

Table 9 presents the average channel gains and RMS delay spreads (i.e. averaged over 100 cells in the room) for D1, D2, D3, D4, D5, D6 and D7. It is observed from table 9 that the best location of photodetector (i.e. minimum path loss) is D5. It can also be noted that D1, D2, D3, D4, D5 and D6 have similar channel gain values in the range of 6×10^{-6}–7.19×10^{-6}. In comparison to them, D7 has about 2.95×10^{-6}–4.41×10^{-6} less channel gain on average since there is no LOS component.

In figure 23, we present the cumulative distribution function (CDF) of path loss as seen by the individual photodetectors Dn , $n = 1, \ldots, 7$. This defines the probability that path loss will

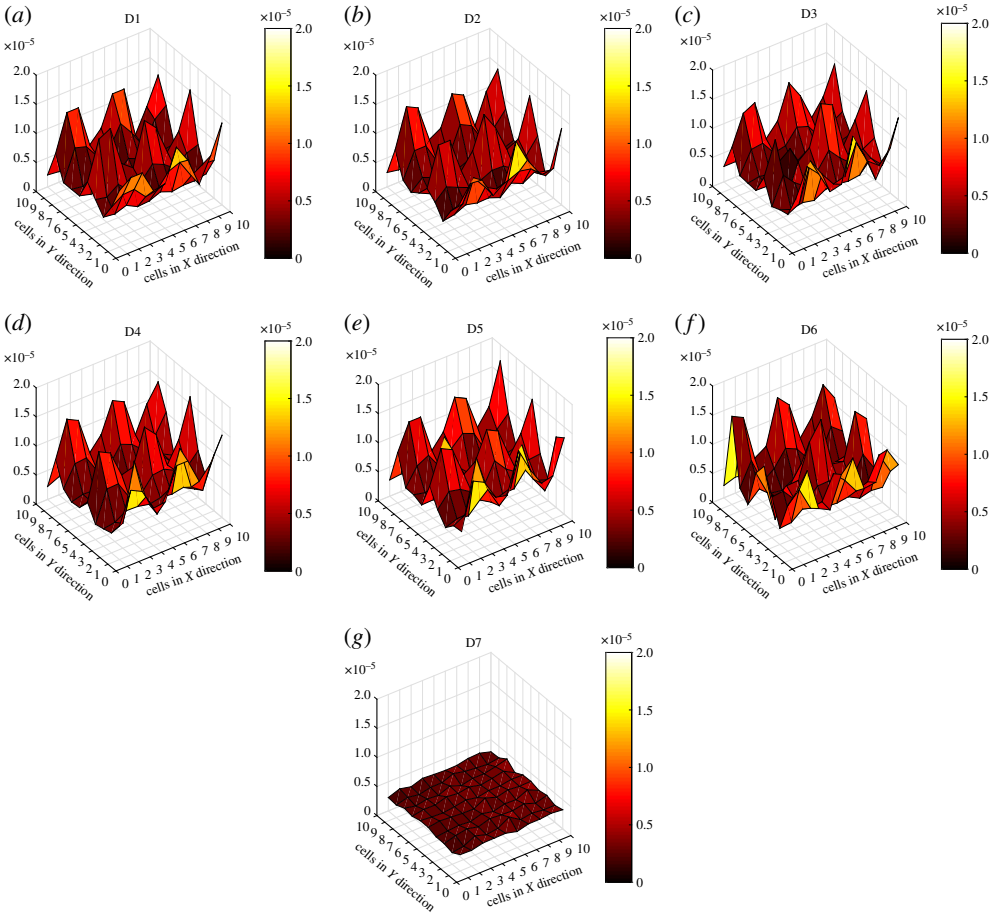

Figure 22. Spatial distributions of path loss as seen by the individual photodetectors *Dn*, $n = 1, \ldots, 7$. (Online version in colour.)

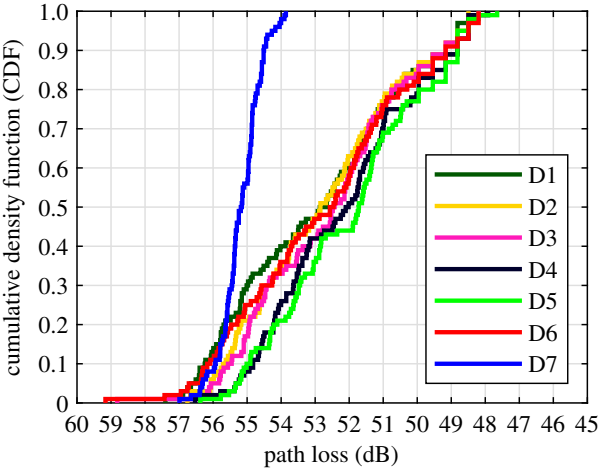

Figure 23. CDF of path loss as seen by the individual photodetectors *Dn*, $n = 1, \ldots, 7$. (Online version in colour.)

take less than or equal to a specific value. The figure further confirms the similar performance behaviours of D1, D2, D3, D4, D5 and D6 locations.

6. Conclusion and discussions

The propagation channel dictates the fundamental limits on the performance of any communication system. Realistic channel modelling is therefore a critical step for design, analysis and testing of VLC systems. In the first part of the paper, we provided an overview of channel modelling approaches including both deterministic and non-deterministic approaches in an effort to provide a tutorial discussion in the relatively new field of VLC channel modelling. A comparative discussion of various recursive, geometric-based and MCRT studies was presented emphasizing the underlying assumptions and pointing out advantages/disadvantages of each approach.

In the second part of the paper, we elaborated on the site-specific channel modelling approach based on non-sequential ray tracing. Using this approach, we obtained sample CIRs for a typical indoor environment with multiple light sources. It was observed that multiple LOS components might be present in the CIR due to the availability of multiple sources. Based on the distances between light sources and receiver locations, some of these LOS components are not resolvable. We further investigated the effect of higher-order reflections, which highly depends on the type of reflections. Our results demonstrated that while higher order reflections larger than four is negligible for a typical room size assuming diffuse reflections, up to eight reflections should be considered for a more precise characterization under the assumption of mostly specular reflections.

We further presented reference channel models for representative scenarios such as workplace, living room and manufacturing cell developed through this approach and endorsed by the IEEE. These models were used as guidelines for physical layer design in the ongoing IEEE standardization work on VLC (IEEE 802.15.13) [34]. For example, large variations in channel gains with respect to test point locations are observed in reference scenario 1. Such changes necessitate the use of link adaptation techniques (i.e. transmission parameters such as modulation type/size, transmit power etc. are selected according to channel conditions) which are now part of the IEEE 802.15.13 standard draft [34]. It was also observed that RMS delay spreads in these reference scenarios vary between 10 and 15 ns. If high data rates (in the order of tens of MHz) are considered, this will result in ISI and requires the use of either time-domain equalization or OFDM-based multicarrier transmission techniques. That has indeed become the motivation for the selection of DCO-OFDM as the mandatory PHY layer design choice in IEEE 802.15.13 [34].

In the third and last part, we investigated the effect of photodetector location/orientation for a mobile user. For this purpose, we considered a mobile receiver terminal in the form of a cell phone with seven possible locations for the photodetector. Five of these are on the top edge and two of them are on the top round corners of the device. The user holds the phone in his hand next to his ear with 45° rotation upward. Our results demonstrated that as user moves within the room, the spatial distributions of channel gain follow sinusoidal-like patterns. When the user approaches a luminaire, the signal strength increases and the maximum value of channel gain occurs when the user is right under the luminaire. When the user walks away, the signal strength decreases. Our results further provide insight on the choice of photodetector location for maximizing the signal strength. It was particularly observed that the top side of the phone is most favourable as PD location due to the fact that the channel DC gain is maximized.

Data accessibility. This article has no additional data.

Authors' contributions. F.M. performed the computer simulations and wrote the first draft of the paper. M.U. devised the main conceptual idea, supervised the simulation study and contributed to the writing of the paper.

Competing interests. We declare we have no competing interests.

Funding. This work was supported by the Turkish Scientific and Research Council (TUBITAK) under grant no. 215E311.

References

1. Uysal M. 2019 Visible light communications: from theory to industrial standardization. In *Optical Fiber Communication Conf., Optical Society of America, San Diego, CA, 3–7 March*, pp. Th3I-4. Washington, DC: OSA.
2. Dimitrov S, Haas H. 2015 *Principles of LED light communications: towards networked Li-Fi*, 1st edn. Cambridge, UK: Cambridge University Press.
3. Uysal M, Capsoni C, Ghassemlooy Z, Boucouvalas A, Udvary E. 2016 *Optical wireless communications: an emerging technology.* Berlin, Germany: Springer.
4. Chi N. 2018 *LED-based visible light Communications*. Berlin, Germany: Springer.
5. Al-Kinani A, Wang CX, Zhou L, Zhang W. 2018 Optical wireless communication channel measurements and models. *IEEE Commun. Surv. Tuts.* **20**, 1939–1962. (doi:10.1109/COMST.2018.2838096)
6. Luo J, Fan L, Li H. 2017 Indoor positioning systems based on visible light communication: state of the art. *IEEE Commun. Surv. Tuts.* **19**, 2871–2893. (doi:10.1109/COMST.2017.2743228)
7. Qiu Y, Chen HH, Meng WX. 2016 Channel modelling for visible light communications—a survey. *Wirel. Commun. Mob. Comput.* **16**, 2016–2034. (doi:10.1002/wcm.2665)
8. Karunatilaka D, Zafar F, Kalavally V, Parthiban R. 2015 LED based indoor visible light communications: state of the art. *IEEE Commun. Surv. Tuts.* **17**, 1649–1678. (doi:10.1109/COMST.2015.2417576)
9. Pathak PH, Feng X, Hu P, Mohapatra P. 2015 Visible light communication, networking, and sensing: a survey, potential and challenges. *IEEE Commun. Surv. Tuts.* **17**, 2047–2077. (doi:10.1109/COMST.2015.2476474)
10. Jovicic A, Li J, Richardson T. 2013 Visible light communication: opportunities, challenges and the path to market. *IEEE Commun. Mag.* **51**, 26–32. (doi:10.1109/MCOM.2013.6685754)
11. O'Brien DC. 2011 Visible light communications: challenges and potential. In *Proc. IEEE Photonics Conf. (PHO), 24th Annual Meeting, Arlington, VA*, pp. 365–366. Piscataway, NJ: IEEE.
12. O'Brien DC, Zeng L, Le-Minh H, Faulkner G, Walewski JW, Randel S. 2008 Visible light communications: Challenges and possibilities. In *Proc. IEEE 19th Int. Symp. Personal Indoor and Mobile Radio Communications (PIMRC), Cannes, France*, pp. 1–5. Piscataway, NJ: IEEE.
13. Rajagopal S, Roberts RD, Lim S-K. 2012 IEEE 802.15.7 visible light communication: modulation schemes and dimming support. *IEEE Commun. Mag.* **50**, 72–82. (doi:10.1109/MCOM.2012.6163585)
14. Park S, Jung D, Shin H, Shin D, Hyun Y, Lee K, Oh Y. 2007 Information broadcasting system based on visible light signboard. In *Proc. Wireless Optical Communication, Montreal, Canada, 30 May–1 June*, pp. 311–313. Anaheim, CA: ACTA Press.
15. Komine T, Nakagawa M. 2004 Fundamental analysis for visible light communication system using LED lights. *IEEE Trans. Consum. Electron.* **50**, 100–107. (doi:10.1109/TCE.2004.1277847)
16. Bian R, Tavakkolnia I, Haas H. 2019 15.73 Gb/s visible light communication with off-the-shelf LEDs. *J. Lightw. Technol.* **37**, 2418–2424. (doi:10.1109/JLT.2019.2906464)
17. Mossaad MS, Hranilovic S, Lampe L. 2015 Visible light communications using OFDM and multiple LEDs. *IEEE Trans. Commun.* **63**, 4304–4313. (doi:10.1109/TCOMM.2015.2469285)
18. Dissanayake SD, Armstrong J. 2013 Comparison of ACO-OFDM, DCO-OFDM and ADO-OFDM in IM/DD systems. *J. Lightw. Technol.* **31**, 1063–1072. (doi:10.1109/JLT.2013.2241731)
19. Fernando N, Hong Y, Viterbo E. 2012 Flip-OFDM for unipolar communication systems. *IEEE Trans. Commun.* **60**, 3726–3733. (doi:10.1109/TCOMM.2012.082712.110812)
20. Narmanlioglu O, Kizilirmak RC, Baykas T, Uysal M. 2017 Link adaptation for MIMO OFDM visible light communication systems. *IEEE Access* **5**, 26 006–26 014. (doi:10.1109/ACCESS.2017.2771333)
21. Hong Y, Wu T, Chen L-K. 2016 On the performance of adaptive MIMO-OFDM indoor visible light communications. *IEEE Photon. Technol. Lett.* **28**, 907–910. (doi:10.1109/LPT.2016.2517192)
22. Wu L, Zhang Z, Dang J, Liu H. 2015 Adaptive modulation schemes for visible light communications. *J. Lightw. Technol.* **33**, 117–125. (doi:10.1109/JLT.2014.2374171)
23. Na Z, Wang Y, Xiong M, Liu X, Xia J. 2018 Modelling and throughput analysis of an ADO-OFDM based relay-assisted VLC system for 5G networks. *IEEE Access* **6**, 17 586–17 594. (doi:10.1109/ACCESS.2018.2817487)

24. Feng L, Hu RQ, Wang J, Qian Y. 2018 Deployment issues and performance study in a relay-assisted indoor visible light communication system. *IEEE Syst. J.* **13**, 562–570. (doi:10.1109/JSYST.2018.2869073)
25. Kizilirmak RC, Narmanlioglu O, Uysal M. 2015 Relay-assisted OFDM-based visible light communications. *IEEE Trans. Commun.* **63**, 3765–3778. (doi:10.1109/TCOMM.2015.2464815)
26. Wei L, Zhang H, Song J. 2016 Experimental demonstration of a cubic-receiver-based MIMO visible light communication system. *IEEE Photon. J.* **9**, 1–7.
27. Zhu Y-J, Liang W-F, Zhang J-K, Zhang Y-Y. 2015 Space-collaborative constellation designs for MIMO indoor visible light communications. *IEEE Photon. Technol. Lett.* **27**, 1667–1670. (doi:10.1109/LPT.2015.2435009)
28. Fath T, Haas H. 2013 Performance comparison of MIMO techniques for optical wireless communications in indoor environments. *IEEE Trans. Commun.* **61**, 733–742. (doi:10.1109/TCOMM.2012.120512.110578)
29. Ling X, Wang J, Ding Z, Zhao C, Gao X. 2018 Efficient OFDMA for LiFi downlink. *J. Lightw. Technol.* **36**, 1928–1943. (doi:10.1109/JLT.2018.2796120)
30. Li H, Huang Z, Xiao Y, Zhan S, Ji Y. 2019 A power and spectrum efficient NOMA scheme for VLC network based on hierarchical pre-distorted LACO-OFDM. *IEEE Access* **7**, 48 565–48 571. (doi:10.1109/ACCESS.2019.2908524)
31. Ma S, Li H, He Y, Yang R, Lu S, Cao W, Li S. 2018 Capacity bounds and interference management for interference channel in visible light communication networks. *IEEE Trans. Wirel. Commun.* **18**, 182–193. (doi:10.1109/TWC.2018.2878585)
32. Wang Y, Haas H. 2015 Dynamic load balancing with handover in hybrid Li-Fi and Wi-Fi networks. *J. Lightw. Technol.* **33**, 4671–4682. (doi:10.1109/JLT.2015.2480969)
33. Dastgheib MA, Beyranvand H, Salehi JA, Maier M. 2018 Mobility-aware resource allocation in VLC networks using T-step look-ahead policy. *J. Lightw. Technol.* **36**, 5358–5370. (doi:10.1109/JLT.2018.2872869)
34. Uysal M, Miramirkhani F, Narmanlioglu O, Baykas T, Panayirci E. 2017 IEEE 802.15.7r1 reference channel models for visible light communications. *IEEE Commun. Mag.* **55**, 212–217. (doi:10.1109/MCOM.2017.1600872CM)
35. Gfeller FR, Bapst U. 1979 Wireless in-house data communication via diffuse infrared radiation. *Proc. IEEE* **67**, 1474–1485. (doi:10.1109/PROC.1979.11508)
36. Barry JR, Kahn JM, Krause WJ, Lee EA, Messerschmitt DG. 1993 Simulation of multipath impulse response for wireless optical channels. *IEEE J. Sel. Areas Commun.* **11**, 367–379. (doi:10.1109/49.219552)
37. Lopez-Hermandez FJ, Betancor MJ. 1997 DUSTIN: algorithm for calculation of impulse response on IR wireless indoor channels. *IEEE Electron. Lett.* **33**, 1804–1806. (doi:10.1049/el:19971224)
38. Abtahi M, Hashemi H. 1995 Simulation of indoor propagation channel at infrared frequencies in furnished office environments. In *6th IEEE Int. Symp. Personal Indoor and Mobile Radio Communications (PIMRC) Wireless: Merging onto the Information Superhighway*, pp. 306–310. Piscataway, NJ: IEEE.
39. Carruthers JB, Kannan P. 2002 Iterative site-based modelling for wireless infrared channels. *IEEE Trans. Antennas Propag.* **50**, 759–765. (doi:10.1109/TAP.2002.1011244)
40. Carruthers JB, Kahn JM. 1997 Modelling of nondirected wireless infrared channels. *IEEE Trans. Commun.* **45**, 1260–1268. (doi:10.1109/26.634690)
41. Jungnickel V, Pohl V, Nonnig S, Von Helmolt C. 2002 A physical model of the wireless infrared communication channel. *IEEE J. Sel. Areas Commun.* **20**, 631–640. (doi:10.1109/49.995522)
42. Hayasaka N, Ito T. 2007 Channel modelling of nondirected wireless infrared indoor diffuse link. *Electronics and Communications in Japan (Part I: Communications)* **90**, 9–19. (doi:10.1002/ecja.20352)
43. Lopez-Hernandez FJ, Perez-Jimeniz R, Santamaria A. 1998 Monte Carlo calculation of impulse response on diffuse IR wireless indoor channels. *IEEE Electron. Lett.* **34**, 1260–1262. (doi:10.1049/el:19980825)
44. Lopez-Hernandez FJ, Perez-Jimenez R, Santamaria A. 1998 Modified Monte Carlo scheme for high-efficiency simulation of the impulse response on diffuse IR wireless indoor channels. *IEEE Electron. Lett.* **34**, 1819–1820. (doi:10.1049/el:19981173)

45. Chowdhury MS, Zhang W, Kavehrad M. 2014 Combined deterministic and modified Monte Carlo method for calculating impulse responses of indoor optical wireless channels. *J. Lightwave Technol.* **32**, 3132–3148. (doi:10.1109/JLT.2014.2339131)
46. Dimitrov S, Mesleh R, Haas H, Cappitelli M, Olbert M, Bassow E. 2009 On the SIR of a cellular infrared optical wireless system for an aircraft. *IEEE J. Sel. Areas Commun.* **27**, 1623–1638. (doi:10.1109/JSAC.2009.091212)
47. Nguyen HQ, Choi JH, Kang M, Ghassemlooy Z, Kim DH, Lim SK, Kang TG, Lee CG. 2010 A MATLAB-based simulation program for indoor visible light communication system. In *7th IEEE Int. Symp. Communication Systems Networks and Digital Signal Processing (CSNDSP), July 2010, Newcastle upon Tyne*, pp. 537–540. Piscataway, NJ: IEEE.
48. Long S, Khalighi MA, Wolf M, Bourennane S, Ghassemlooy Z. 2014 Channel characterization for indoor visible light communications. In *IEEE 3rd Int. Workshop on Optical Wireless Communications (IWOW), Funchal, Portugal, September 2014*, pp. 75–79. Piscataway, NJ: IEEE.
49. Lee K, Park H, Barry JR. 2011 Indoor channel characteristics for visible light communications. *IEEE Commun. Lett.* **15**, 217–219. (doi:10.1109/LCOMM.2011.010411.101945)
50. Ding J, Chih-Lin I, Xu Z. 2016 Indoor optical wireless channel characteristics with distinct source radiation patterns. *IEEE Photon. J.* **8**, 1–15.
51. Schulze H. 2016 Frequency-domain simulation of the indoor wireless optical communication channel. *IEEE Trans. Commun.* **64**, 2551–2562. (doi:10.1109/TCOMM.2016.2556684)
52. Chen C, Basnayaka D, Haas H. 2016 Non-line-of-sight channel impulse response characterization in visible light communications. In *IEEE Int. Conf. Communications (ICC), Kuala Lumpur, Malaysia, May 2016*, pp. 1–6. Piscataway, NJ: IEEE.
53. Al-Kinani A, Wang CX, Haas H, Yang Y. 2016 Characterization and modeling of visible light communication channels. In *IEEE 83rd Vehicular Technology Conf. (VTC Spring), Nanjing, China, May 2016*, pp. 1–5. Piscataway, NJ: IEEE.
54. Al-Kinani A, Wang CX, Haas H, Yang Y. 2016 A geometry-based multiple bounce model for visible light communication channels. In *IEEE Wireless Communications and Mobile Computing Conf. (IWCMC), Paphos, Cyprus, September 2016*, pp. 31–37. Piscataway, NJ: IEEE.
55. Rodriguez SP, Jimenez RP, Mendoza BR, Hernandez FJL, Alfonso AJA. 2013 Simulation of impulse response for indoor visible light communications using 3D CAD models. *EURASIP J. Wirel. Commun. Netw.* **2013**, 7. (doi:10.1186/1687-1499-2013-7)
56. Rufo J, Rabadan J, Guerra V, Perez-Jimenez R. 2017 BRDF models for the impulse response estimation in indoor optical wireless channels. *IEEE Photon. Technol. Lett.* **29**, 1431–1434. (doi:10.1109/LPT.2017.2723543)
57. Lee HS. 2009 A photon modeling method for the characterization of indoor optical wireless communication. *Prog. Electromagnet. Res.* **92**, 121–136. (doi:10.2528/PIER09030506)
58. Miramirkhani F, Uysal M. 2015 Channel modeling and characterization for visible light communications. *IEEE Photon. J.* **7**, 1–16. (doi:10.1109/JPHOT.2015.2504238)
59. Miramirkhani F, Uysal M, Panayirci E. 2015 Novel channel models for visible light communications. *Broadband Access Commun.* **9387**, 93870Q.
60. Tien CH, Hung CH. 2009 An iterative model of diffuse illumination from bidirectional photometric data. *Opt. Express* **17**, 723–732. (doi:10.1364/OE.17.000723)
61. Marschner SR, Westin SH, Lafortune EP, Torrance KE, Greenberg DP. 1999 Image-based BRDF measurement including human skin. In *Rendering Techniques' 99*, pp. 131–144. Vienna: Springer.
62. Weyrich T, Lawrence J, Lensch HP, Rusinkiewicz S, Zickler T. 2009 Principles of appearance acquisition and representation. *Found. Trends® Comput. Graph. Vis.* **4**, 75–191. (doi:10.1561/0600000022)
63. Zemax OpticStudio knowledgebase, [Online]. See https://my.zemax.com/en-US/Knowledge-Base/kb-article/?ka=KA-01504.
64. 'Zemax OpticStudio optical design software illumination design software'. See http://www.zemax.com/opticstudio.
65. Sivabalan A, John J. 2003 Modeling and simulation of indoor optical wireless channels: a review. In *IEEE Proc. Conf. Convergent Technologies for Asia-Pacific Region, Bangalore, India, 15–17 October*, vol. 3, pp. 1082–1085. Piscataway, NJ: IEEE.
66. Press WH, Teukolsky SA, Vetterling WT, Flannery BP. 2007 *Numerical recipes*. Cambridge, UK: Cambridge University Press.

67. Zemax OpticStudio knowledgebase, [Online]. See https://my.zemax.com/en-US/Knowledge-Base/kb-article/?ka=KA-01413.
68. Miramirkhani F, Narmanlioglu O, Uysal M, Panayirci E. 2017 A mobile channel model for VLC and application to adaptive system design. *IEEE Commun. Lett.* **21**, 1035–1038. (doi:10.1109/LCOMM.2017.2651800)
69. Uysal M, Baykas T, Miramirkhani F, Serafimovski N, Jungnickel V. 2015 TG7r1 channel model document for high-rate PD communications. IEEE 802.15-15/0746r1, September 2015. See https://mentor.ieee.org/802.15/dcn/15/15-15-0746-01-007a-tg7r1-channel-model-document-for-high-rate-pd-communications.pdf.
70. Uysal M, Miramirkhani F, Baykas T, Serafimovski N, Jungnickel V. 2015 LiFi Channel Models: Office, Home and Manufacturing Cell. IEEE 802.15-15/0685r0, September 2015. [Online]. See https://mentor.ieee.org/802.15/dcn/15/15-15-0685-00-007a-lifi-reference-channel-models-office-home-manufacturing-cell.pdf.
71. Lighting of indoor work places. International Standard. See https://www.iso.org.
72. pureLiFi, [Online]. See http://purevlc.co.uk/li-fire/purevlc-li-1st/.
73. Signify, [Online]. See https://www.signify.com/b-dam/signify/en-aa/about/news/2019/20190619-signify-launches-trulifi/20190619-Signify-launches-Trulifi.pdf.
74. Narmanlioglu O, Turan B, Kizilirmak RC, Ergen SC, Uysal M. 2018 SC-FDE based MIMO uplink transmission over infrared communication channels. In *IEEE 88th Vehicular Technology Conf. (VTC-Fall)*, pp. 1–5. Piscataway, NJ: IEEE.
75. Komine T, Nakagawa M. 2004 A study of shadowing on indoor visible-light wireless communication utilizing plural white LED lightings. In *1st Int. Symp. Wireless Communication Systems, Mauritius*, pp. 36–40. Piscataway, NJ: IEEE.
76. Komine T, Haruyama S, Nakagawa M. 2005 A study of shadowing on indoor visible-light wireless communication utilizing plural white LED lightings. *Wirel. Pers. Commun.* **34**, 211–225. (doi:10.1007/s11277-005-8734-x)
77. Xiang Y, Zhang M, Kavehrad M, Chowdhury MS, Liu M, Wu J, Tang X. 2014 Human shadowing effect on indoor visible light communications channel characteristics. *Opt. Eng.* **53**, 086113. (doi:10.1117/1.OE.53.8.086113)
78. Chvojka P, Zvanovec S, Haigh PA, Ghassemlooy Z. 2015 Channel characteristics of visible light communications within dynamic indoor environment. *J. Lightwave Technol.* **33**, 1719–1725. (doi:10.1109/JLT.2015.2398894)
79. Tsonev D *et al.* 2016 Low-bandwidth LiFi PHY & MAC. May 2016. See https://mentor.ieee.org/802.15/dcn/16/15-16-0363-00-007a-text-input-lifi-low-bandwidth-phy-and-mac-d0.docx.